

RevaMp3D: Architecting the Processor Core and Cache Hierarchy for Systems with Monolithically-Integrated Logic and Memory

Nika Mansouri Ghiasi¹ Mohammad Sadrosadati¹ Geraldo F. Oliveira¹ Konstantinos Kanellopoulos¹
 Rachata Ausavarungnirun² Juan Gómez Luna¹ João Ferreira¹ Jeremie S. Kim¹ Christina Giannoula^{1,3}
 Nandita Vijaykumar³ Jisung Park⁴ Onur Mutlu¹

¹ETH Zürich

²MangoBoost

³University of Toronto

⁴POSTECH

Abstract

Recent nano-technological advances enable the *Monolithic 3D (M3D)* integration of multiple memory and logic layers *in a single chip*. Such integration enables fine-grained and high-bandwidth connections between layers, which significantly alleviates main memory bottlenecks. We show for a variety of workloads, on a state-of-the-art M3D-based system, that the performance and energy bottlenecks shift from main memory to the processor core and cache hierarchy. Therefore, to effectively utilize the chip’s area, given the applications’ shifted requirements, there is a need to revisit current processor core and cache hierarchy designs that have been conventionally tailored to tackle the memory bottleneck. Based on the insights from our design space exploration, we propose **RevaMp3D**, which introduces five key changes to the state-of-the-art M3D-based system. First, we propose removing the shared last-level cache, based on our observation that doing so achieves speedups on par with, or even exceeding, speedups achieved by increasing its size or reducing its latency, across all our workloads (even for ones with high last-level cache hit rates). Second, since our analysis shows that improving L1 cache latency has a large impact on performance in M3D-based systems, we reduce L1 cache latency by leveraging an M3D layout that reduces its wire lengths. Third, we leverage the area reclaimed from removing large caches to widen and scale up various structures in the processor pipeline that enable greater instruction-level parallelism (e.g., reorder buffer and execution units). This design accommodates more in-flight requests, which can be efficiently served due to the high M3D memory bandwidth. To avoid latency penalties from these larger structures, we leverage M3D layouts that keep their wire lengths short. Fourth, to facilitate high thread-level parallelism, we propose a new fine-grained synchronization technique, using M3D technology’s dense inter-layer connectivity, to improve inter-thread communication. Fifth, we leverage the M3D main memory to mitigate the performance and energy bottlenecks of the processor core. To this end, we propose a processor frontend design that memoizes the repetitive fetched, decoded, and reordered instructions, stores them in main memory at low cost, and turns off the relevant parts of the processor core when possible. The high-bandwidth, energy-efficient M3D memory enables storing and loading the memorized instructions efficiently, thus eliminating the need for large SRAM capacity for storing the memorized instructions. Our evaluation using a wide range of 20 real-world workloads and 7 multi-programmed mixes shows that by re-architecting the M3D-based system by targeting its shifted bottlenecks and taking advantage of its unique opportunities, RevaMp3D provides 1.2×–2.9× speedup and 1.2×–1.4× energy reduction, while achieving 12.3% smaller area, compared to the state-of-the-art M3D-based system. Compared to the state-of-the-art 3D and 2D systems, RevaMp3D provides 4.96× and 7.14×

average speedup, respectively. As part of our design space exploration, we also analyze the impact of RevaMp3D’s design decisions for M3D-based systems with various main memory latency values since memory latency can vary depending on the design decisions made to meet certain requirements of the target system. This analysis facilitates making the appropriate design decisions based on M3D main memory latency, thereby benefiting a wide range of workloads.

1 Introduction

Recent nano-technological advances enable the *Monolithic 3D (M3D)* integration of multiple logic and memory layers on a single chip [1–11]. M3D integration is a promising technology to alleviate the memory bottleneck that significantly limits the performance and energy efficiency of data-intensive applications in conventional systems. M3D integration enables significantly higher main memory bandwidth compared to other 3D integration technologies, such as Through Silicon Via (TSV)-based [8, 12–14] or hybrid bonding-based [15–20] integrations. This is due to M3D’s much higher density of Inter-Layer Vias (ILVs) that connect different device layers. M3D integration can also lead to lower main memory latency by exploiting the fine-grained ILVs to efficiently enable (i) a large number of memory channels, each connected to relatively small memory arrays with shorter wire lengths, (ii) fine-grained 3D layout of the memory array to further shorten the wires, and (iii) low-latency interconnections between logic and memory layers on the same chip.

Due to its benefits, M3D integration has received substantial interest in both academia (e.g., [1–11, 21–27]) and industry (e.g., [28–33]). Several prior works propose improvements for M3D-based systems, mainly focusing on three aspects. First, at the device and circuit levels, various works (e.g., [3, 10, 34–49]) propose improvements to the logic and memory components and their integration in M3D substrates. Second, at the architecture level, some works (e.g., [14, 50–56]) demonstrate the impact of the M3D integration of logic layers on the performance and energy efficiency of logic components, such as SRAM structures in processor cores and networks on chips. Other works (e.g., [10, 52]) explore the memory system challenges in M3D (e.g., designing main memory array structures and controllers). Third, at the application level, various works (e.g., [51, 57–63]) propose application-specific M3D accelerators.

While prior works propose various improvements for M3D-based systems, no prior work re-examines the processor core and cache hierarchy designs based on the requirements of real-world applications on systems with monolithically-integrated logic and memory. Therefore, to effectively leverage M3D integration’s benefits, it is important to understand its implications on the performance and

energy bottlenecks of real-world applications. These implications can then guide re-examining processor core and cache hierarchy designs. Based on our experimental analysis of a variety of workloads simulated on a state-of-the-art M3D-based system [5, 7–9], we make two key observations. First, compared to the 2D and 3D systems, performance bottlenecks in the M3D-based system *shift* substantially from the main memory to the processor core and caches (even for the memory-bound workloads). Second, the processor core becomes the primary source of energy consumption due to the more energy-efficient M3D main memory (see §2).

Our goal in this work is to design the core and cache hierarchy given the shifted bottlenecks in M3D systems. To this end, we take two steps. First, we explore the implications of shifted bottlenecks on the processor core and cache hierarchy design. Second, based on these implications and by leveraging the new opportunities of M3D integration, we design a new M3D-based system.

Implications of M3D Integration on Cache Hierarchy Design.

Through a detailed analysis of the *depth*, *size*, and *latency* of the cache hierarchy in an M3D-based system, we make three new observations. First, all evaluated workloads perform better or equally well in an M3D-based system with a shallow one-level cache hierarchy (i.e., with L1 caches) compared to an M3D-based system with a deeper and larger cache hierarchy (§5.1.1). Second, although M3D integration enables reducing cache latency, the benefit of removing the deeper cache levels is still higher than or comparable to increasing the sizes (§5.1.2) and/or improving the latencies of the deeper cache levels (§5.1.3). Third, in contrast to the deeper levels of the cache hierarchy, L1 caches in an M3D-based system are still critical for performance, and improving their latency improves performance for a wide range of workloads (§5.1.3).

Implications of M3D Integration on Processor Core Design.

We perform a detailed analysis of different units in all stages of an out-of-order superscalar processor core pipeline. We highlight three new observations, demonstrating the most important factors impacting performance. First, larger pipeline widths improve M3D performance since they increase the number of in-flight requests, which can be effectively served given M3D’s high memory bandwidth (§5.2.1). Second, the performance impact of pipeline frontend (e.g., fetch, decode, and branch prediction units) increases significantly (§5.2.3), as M3D shifts the bottleneck away from memory, increasing the fraction of execution time dominated by these units. Third, while high-bandwidth main memory enables running many threads concurrently, the overhead of synchronization between threads in multi-threaded workloads limits performance (§5.2.4).

Re-Architecting M3D. Considering the implications of M3D integration on cache hierarchy and processor core design, we propose an optimized M3D-based system, *RevaMp3D*, based on five key design decisions. First, we remove the shared last-level cache (L2 in our M3D baseline) from the cache hierarchy. Second, we reduce L1 cache latency by devising a 3D layout for the SRAM array, in which the array is divided across two logic layers to reduce its overall wire lengths and latency. Third, we leverage the area reclaimed from removing the large cache to widen and scale up various structures in the processor pipeline that enable greater instruction-level parallelism (e.g., reorder buffer and execution units). This design accommodates more in-flight requests, which can be efficiently served

due to the high M3D memory bandwidth. We avoid latency penalties from these larger structures by leveraging M3D layouts to keep their wire lengths short. Both the second and third design decision take advantage of the dense ILVs that enable efficient vertical layout of the processor structures [14, 50, 51, 53–56]. Fourth, we introduce a new fine-grained register file-level synchronization technique, which eliminates the additional latency in the memory hierarchy for synchronization. This technique is realized by using the thin ILVs to efficiently increase the register file bandwidth to support both the regular operand accesses and the synchronization-related accesses. Fifth, we leverage the M3D main memory to mitigate the performance and energy bottlenecks of the processor core. To this end, we propose a processor frontend design that memoizes the repetitive (i.e., in a loop) fetched, decoded, and reordered instructions, stores them in main memory at low cost, and turns off the relevant parts of the processor core when possible. The high-bandwidth, energy-efficient M3D main memory enables storing and loading the memorized instructions efficiently, thus eliminating the area overhead of prior memoization techniques that require a large SRAM capacity [64, 65]. This design alleviates (i) energy bottlenecks when repeated instructions execute, and (ii) branch misprediction overhead since a large fraction of instructions do not need to be fetched, decoded, and re-ordered on branch misprediction.

Key Results. We evaluate *RevaMp3D* using a heavily modified cycle-accurate architectural simulator (ZSim [66]) to flexibly explore various designs and faithfully model the M3D-based systems. We experimentally calibrate the parameters for the M3D baseline based on the fabricated device models, circuit analysis, interconnect model, and physical design tools presented in [9]. We evaluate *RevaMp3D* using a wide range of 20 real-world workloads and 7 multi-programmed mixes. On systems with 1, 16, 64, and 128 cores, *RevaMp3D* provides 1.2×–2.9× speedup and 1.2×–1.4× energy reduction across all evaluated workloads and core counts, with a 12.3% reduction in logic area, compared to the state-of-the-art M3D-based system [1, 9], while providing 4.96× and 7.14× average speedup compared to the state-of-the-art 3D and 2D systems, respectively. As part of our design space exploration, we analyze the impact of *RevaMp3D*’s design decisions for M3D-based systems with various main memory latency values since memory latency can vary depending on the design decisions made to meet certain requirements of the target system. This analysis facilitates making the appropriate design decisions based on the M3D main memory latency. Our analysis demonstrates that by re-architecting M3D systems based on their shifted bottlenecks and unique opportunities provided by M3D integration, we can re-allocate the logic area to different units in the processor core and cache hierarchy more efficiently, thereby benefiting a wide range of workloads.

This work makes the following **key contributions**:

- We conduct a rigorous design space exploration of key components of the processor core and cache hierarchy to understand the implications of the M3D integration of logic and memory layers on the applications’ performance and energy bottlenecks.
- We introduce *RevaMp3D*, an optimized M3D-based system, based on our insights from our analysis and leveraging M3D integration’s opportunities, such as tightly-integrated logic layers and fast and energy-efficient main memory.

- We show that RevaMp3D provides significant performance improvement and energy reduction compared to the state-of-the-art M3D-based system, while achieving a smaller logic area.

2 M3D Technology

We provide a brief overview of the M3D integration technology, state-of-the-art M3D-based systems, and their technology feasibility and constraints.

M3D Integration Technology. There has been significant effort into enabling tighter integration of logic and memory layers in the system to improve performance and energy. Fig. 1 compares three different systems. In 2D systems, computation and memory units are connected via off-chip links with low bandwidth, which is imposed by the limited number of I/O pins in the memory system. In 3D systems [15–20, 67–74], memory layers are connected using Through-Silicon Vias (TSVs) or hybrid bonding and can be connected to logic units directly below the memory layers using TSVs/hybrid bonding or on an interposer substrate. Compared to 2D systems, 3D systems provide higher main memory bandwidth, lower latency, and better energy efficiency. In M3D-based systems [1–3, 5–10], logic and memory layers are *monolithically-fabricated on the same chip* with a large number of thin Inter-Layer Vias (ILVs) with very small pitch sizes (e.g., <100 nm [1, 9, 14]). Compared to TSV, which has a pitch size of $\sim 2.6\text{--}25\ \mu\text{m}$ [14, 75], and hybrid bonding, which has a pitch size of $\sim 0.3\text{--}10\ \mu\text{m}$ [15–20], the smaller pitch size of ILVs enables a much denser inter-layer connectivity.

There are two classes of M3D-based systems: (i) *only* with logic layers and (ii) with *both* logic and memory layers. The first type provides several optimization opportunities, such as efficient 3D partitioning of logic structures (e.g., caches, NoCs) to reduce their latency by shortening the wires [14, 50]. The second type enables additional benefits by significantly alleviating the main memory bottlenecks [1, 9, 76, 77]. In this work, we consider the second type. High memory bandwidth is realized by the dense ILVs between logic and memory layers. Low memory latency is achieved due to three reasons. First, the high-bandwidth ILVs enable efficiently devising a large number of memory channels, each connected to relatively small memory arrays. The smaller wire lengths in these arrays lower overall access latency, and the larger channel counts lower the contention across concurrent memory accesses. Second, the low pitch size of the ILVs enables efficient M3D layouts of memory arrays (e.g., placing different banks in a memory channel in different layers). This allows further reduction of wire lengths in a

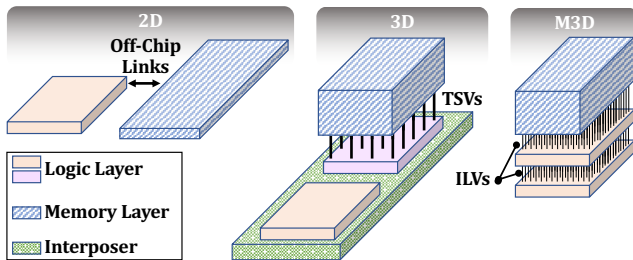


Fig. 1: Systems with 2D, 3D, and M3D integration.

memory array and, subsequently, reduction in the array’s latency.¹ Third, short and dense ILVs lead to low-latency interconnection between logic and memory on the same chip.

Baseline Architecture. We use N3XT [1, 5, 7–9], a state-of-the-art M3D-based system, as our baseline. N3XT leverages emerging technologies such as carbon-nanotube-based transistors in the logic layer [2, 5, 7] and latency-optimized monolithic 3D RRAM arrays in the memory layers [78, 79]. The fabrication and thermal feasibility of the N3XT architecture has been demonstrated by real prototypes [7]. Fig. 2 shows the baseline M3D architecture [9], integrating several logic layers (one for processor cores, one for cache access circuitry, one for shared L2 cache, two for network on chip to enable high-bandwidth communication between main memory and cores, one for memory access circuitry and memory controllers) and memory layers (64 RRAM layers).

In this work, although we use N3XT as our baseline M3D-based system, we primarily focus on characteristics such as main memory bandwidth and latency rather than device-specific features. Because we evaluate M3D-based systems using a range of parameters (e.g., main memory latency), our insights can be broadly applied to enhance performance and energy efficiency in M3D-based systems that employ different logic and memory device technologies.

Technological Feasibility and Constraints. Prior work shows that both logic and memory layers in N3XT can be fabricated at *low temperatures* (<300°C [1, 9]). This paves the way to fabricating layers monolithically on top of each other in the same chip without the top layers melting the lower layers during fabrication. Some recent works even demonstrate the feasibility of M3D fabrication using commercial silicon facilities [1, 87]. Such works facilitate the wider adoption of M3D integration technology by alleviating the need to devise completely new fabrication lines for M3D. Despite all the benefits, there are two key challenges and constraints for M3D fabrication. First, since the M3D fabrication process is sequential (i.e., device layers need to be monolithically and sequentially integrated on top of each other, as opposed to 3D-stacked devices where layers can be fabricated in parallel), M3D technology suffers from concerns typically regarding increased cost and reduced yield. Second, RRAM, the memory technology used in the baseline M3D-based system considered in this work, has limited write endurance. N3XT addresses this issue using online data relocation wear-leveling, extending the device lifetime to at least 10 years [9]. We incorporate the same solution in our evaluations (§3). We consider the investigation of more efficient solutions (e.g., [88, 89]) for addressing device challenges as a critical and orthogonal direction.

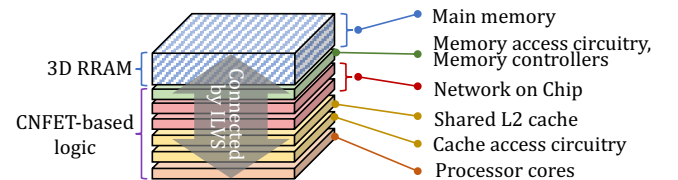


Fig. 2: Overview of the baseline M3D-based system [9].

¹Note that larger pitch sizes of other 3D integration technologies reduce the benefits of fine-grained 3D partitioning of memory arrays [14].

3 Methodology

We describe the workloads and the experimental setup we use in our analysis.

3.1 Workloads

Table 1 summarizes the wide range of multi-threaded workloads used in our analysis, selected from the DAMOV benchmark suite for main memory data movement studies [90]. These workloads are from various domains and pressure different parts of the system. To gain an initial understanding of our workload’s primary bottlenecks, we perform a *top-down analysis* [91], a widely-adopted approach that hierarchically characterizes the workload bottlenecks [91–94]. We use the Intel VTune Profiler [95] to perform the top-down analysis. For each workload, Table 1 shows the backend-bound (BE), DRAM-bound (Mem), and DRAM bandwidth-bound (BW) values obtained from VTune, while running on Intel Xeon E3-1240 processor with 4 cores. BE accounts for the percentage of execution time during which the processor cannot issue new instructions due to stalls at the pipeline backend, including stalls due to memory requests and core execution (e.g., no empty free slot in the execution unit of the pipeline). The stall due to memory requests further divides into stalls due to caches or DRAM (Mem). Mem can be further split into DRAM latency- and bandwidth-bound (BW). Table 1 also shows Last-to-First Miss Ratio (LFMR), a metric proposed for showing the effectiveness of caches [90], which is obtained by dividing the number of L2 cache misses (last-level cache in our M3D baseline) by the number of L1 cache misses. A high LFMR suggests that the L2 cache does not provide significant benefits in reducing the miss rate. We consider LFMR above 90% as high, as most requests are not serviced by the L2 cache.

Based on this characterization, we classify the workloads into three categories: *main memory bandwidth-bound*, *main memory latency-bound*, and *compute-bound*. We categorize the workloads with large BE (>40%), Mem (>40%), and BW (>50%) as DRAM bandwidth-bound since we observe large performance improvements when

improving the main memory bandwidth for these workloads. We categorize workloads with high BE and Mem and low BW as DRAM latency-bound since we observe large performance improvements when improving the main memory latency for these workloads. We categorize workloads with high BE and low Mem as compute-bound. When a workload nearly misses the border between main memory-/compute-bound, we use LFMR to classify the workload as memory-bound (LFMR>90%) or compute-bound.

For our end-to-end evaluations, we also evaluate a wide range of multi-programmed workload mixes, with a focus on combining workloads with various bottlenecks. We summarize the multiprogram workload mixes in Table 2.

Table 2: Workloads used in our analysis.

Class	Mix	Workloads
Memory-bound + Compute-bound	1	Components + 3mm
	3	MIS + atax
	6	PageRank + 2mm
Memory-bound + Memory-bound	7	Triangle + gemm
	5	Oceanncp + StreamCluster
Compute-bound + Compute-bound	2	gemm + atat
	4	NW + 3mm

3.2 Experimental Setup

Modeled Systems. We use a cycle-accurate architectural simulator (ZSim [66]) to flexibly explore various designs and faithfully model the following systems:

- **2D:** a system based on the 2D integration of computation and memory, where the cores and main memory (DRAM) communicate through an off-chip bus.
- **3D:** a system that uses TSVs to integrate memory layers, which connect to compute units via interposers (e.g., [13]). We consider

Table 1: List of workloads and their input sizes.

Class	Workload	Suite	Domain	Input Size (MB)	BE(%)	Mem (%)	BW (%)	ILP	LFMR
Bandwidth-bound	YOLO	Darknet [80]	Machine Learning	204	94.17	62.01	56.60	2.25	0.99
	BFS	Ligra [81]	Graph Processing	2017	44.94	59.14	40.56	1.71	0.98
	BC	Ligra [81]	Graph Processing	2017	75.72	65.16	56.84	2.09	0.99
	KCore	Ligra [81]	Graph Processing	2017	94.54	44.88	78.68	1.62	0.99
	MIS	Ligra [81]	Graph Processing	2017	86.70	71.72	90.88	2.02	0.99
	PageRank	Ligra [81]	Graph Processing	2017	86.70	71.72	90.88	2.02	0.99
	Radii	Ligra [81]	Graph Processing	2017	54.12	43.10	66.34	1.78	0.99
Latency-bound	Copy	STREAM [82]	Benchmarking	3200	80.94	73.98	88.54	2.25	1
	StreamCluster	Rodinia [83]	Data Mining	67	63.84	43.22	17.38	1.74	0.99
	ResNet	Darknet [80]	Machine Learning	230	62.66	55.00	26.74	2.25	0.99
	Oceanncp	Splash-2 [84]	HPC	17	92.98	47.02	22.12	6.63	1
	Components	Ligra [81]	Graph Processing	2017	50.94	42.12	6.62	1.38	0.99
	Triangle	Ligra [81]	Graph Processing	2017	62.08	51.10	18.74	1.41	0.99
	Myocyte	Rodinia [83]	Simulation	364	93.44	89.26	29.92	1.88	0.99
Compute-bound	3mm	PolyBench [85]	Linear Algebra	128	60.3	13.8	34.68	2.75	0.61
	2mm	PolyBench [85]	Linear Algebra	128	62.50	13.8	35.29	2.55	0.60
	atax	PolyBench [85]	Linear Algebra	512	25.50	1.60	14.9	2.37	0.51
	gemm	PolyBench [85]	Linear Algebra	96	63.4	13.8	23.11	2.55	0.58
	ferret	PARSEC [86]	Similarity Search	47	29.22	4.5	0.5	2.64	0.61
	Needleman-Wunsch	Rodinia [83]	Bioinformatics	4295	79.96	39.66	65.46	2.35	0.52

Table 3: 2D, 3D, and M3D system configurations.

System	M3D	3D	2D
Main Memory	64 GB on-chip 3D RRAM [9]; Up to 16 TB/s [9]; FR-FCFS scheduling; 5/13ns R/W (up to 5/60ns R/W); 0.8/1.1 pJ/bit R/W [9]	64 GB on-chip 3D-stacked DRAM using 5um TSVs; HBM2 interface, 1.5 TB/s [12, 13]; FR-FCFS scheduling; 51/55ns R/W; 9 pJ/bit [9]	64 GB off-chip DRAM; DDR4 interface, 102 GB/s [96]; FR-FCFS scheduling; 65/60ns R/W [9]; 20pJ/bit R/W [97]
L3	None	None	Shared 8 MB, 16-way, 27-cycle; 945/1904 pJ per hit/miss [98]
L2	Shared 256 KB per core (0/1/8/64 MB) 8-way, 12-cycle (6-cycle); 46/93 pJ per hit/miss	Shared 256 KB per core, 8-way, 12-cycle; 46/93 pJ per hit/miss	Private 256 KB per core, 8-way, 12-cycle; 46/93 pJ per hit/miss
L1	32 KB, 8-way, 4-cycle (2-cycle); 15/33 pJ per hit/miss [98]		
Processor Core	1/16/64/128 out-of-order cores @ 4 GHz; 4-wide pipeline (8-wide); 128-entry reorder buffer (256-entry); Branch predictor: two-level GAs [99] (TAGE-SC-L [100] and ideal predictor with no mispredictions); 0.48 nJ/inst for M3D; 1.5 nJ/inst for 2D and 3D		

six HBM stacks connected to compute units similar to a state-of-the-art 3D system [101].

- **M3D**: a system based on N3XT [1, 5, 7–9], where memory and logic are monolithically fabricated on each other. We experimentally calibrate the M3D-based system parameters based on the fabricated device models, circuit analysis, interconnect model, and physical design tools presented in [9]. The latency of on-chip main memory in the M3D-based system can depend on various factors (e.g., memory capacity, size of each memory array, and length of local and global wires in the memory array). Therefore, to gain comprehensive insights into M3D-based system design implications, we also evaluate M3D-based systems with varying memory latency values in our design space exploration (§5) and end-to-end evaluations (§7). To this end, we rigorously sweep the memory latency values from half the value reported for the baseline M3D configuration up to a latency value similar to the baseline 2D system.

We summarize all system parameters in Table 3.² We also show other configurations analyzed in §5 in parentheses.

Cache and Core. We initially consider the same core and L1 caches for all configurations. 2D has a deeper and larger cache hierarchy compared to 3D and M3D since it has the lowest available memory bandwidth. We consider a cache hierarchy for M3D similar to N3XT [9] (private L1 and shared L2). We consider the same cache hierarchy for 3D. In §5, we study the effects of different cache and core configurations in M3D.

Main Memory. In our analysis, all three systems have large enough main memory capacity to contain the working set of all applications in Table 1.³ Although the main memory in the M3D baseline is RRAM-based and different from DRAM used in 2D and 3D, in our performance analysis, we primarily distinguish memory systems by their bandwidth and latency and not their other device features. As explained in §2, in our evaluations, we employ the same technique used in the M3D baseline for alleviating the reliability and endurance issues of the RRAM-based memory [9].

Network on Chip. The M3D baseline [9] uses the meshes of trees (MoT) [102] scheme to provide a high-bandwidth connection between the cores and the memory controllers. This network supports uniform memory access (UMA) such that each core has the same access latency to any memory channel.

²The main memory latency values in this table refer to average main memory access latency.

³We also discuss the case where data does not fit in one stack in § 8.

4 Motivational Analysis

We conduct an experimental analysis of performance and energy bottlenecks of a variety of workloads on a state-of-the-art M3D-based system.

4.1 Performance Bottlenecks

Our analysis shows that the M3D-based system achieves significant performance improvements compared to the 3D system (on average 2.82× and up to 9.02×, across all our evaluated workloads). To show how the M3D-based system affects the performance bottlenecks of the conventionally main memory-bound workloads, we compare the performance bottlenecks of *memory latency-/bandwidth-bound* workloads. To this end, we extend ZSim [66] by incorporating the top-down bottleneck analysis [91]. We validate our implementation of the top-down analysis in ZSim by comparing its output against those produced by Intel VTune Profiler [95] running on Intel Xeon E3-1240. Our validation shows that the ZSim-based top-down analysis identifies very similar *trends* in bottlenecks as Intel VTune [95], showing a high Pearson correlation value [103] of 93.94% ($P < 0.001$) across our workloads with various behaviors.

Fig. 3 shows the top-down bottleneck breakdown of a representative latency-bound workload, Triangle, when running on different systems (i.e., 2D, 3D, and M3D) and core counts (1/16/64/128). We make two observations. First, M3D improves performance⁴ over the 2D and 3D baselines by up to 6.82× and 1.47×, respectively. Second, in the M3D-based system, we observe a large reduction in the ratio of execution time spent on the backend, compared to 2D and 3D (on average 1.87× and 1.52×, respectively). In this case, we observe a substantial *bottleneck shift* in the system from the backend to the frontend and speculation.

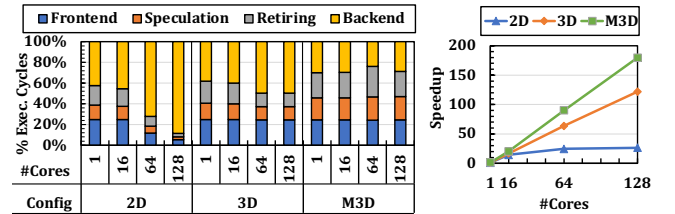


Fig. 3: Bottlenecks of a latency-bound workload (Tri).

⁴Performance refers to the normalized parallel speedup, where all values are normalized against that of the 2D baseline.

Fig. 4 shows the top-down bottleneck breakdown of a representative bandwidth-bound workload, BFS. We observe that, first, M3D improves performance over 2D and 3D by up to 39.63 \times and 4.80 \times across all core counts, respectively. Second, in M3D, we observe 1.57 \times and 1.37 \times reductions in the ratio of execution time spent on the backend compared to 2D and 3D, respectively. To gain a deeper understanding of the backend bottlenecks (which are influenced by the main memory, cache hierarchy, and the processor’s functional units), we study an *idealized* M3D-based system with a one-cycle main memory latency and no main memory bandwidth bottleneck.⁵ We observe that even such a configuration only leads to a 23% speedup, lowering the backend bottleneck only by 5%, which means that the main memory is not a key contributor to the M3D-based system’s backend bottleneck. We conclude that the advancements in M3D memory performance result in substantially *shifting* the application bottlenecks from main memory to other parts of the system.

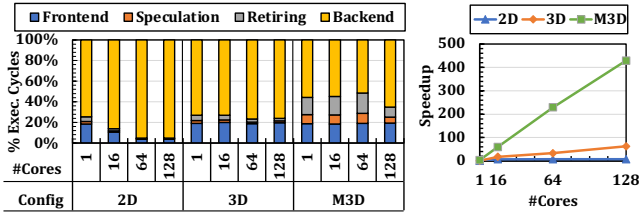


Fig. 4: Bottlenecks of a bandwidth-bound workload (BFS).

4.2 Energy Bottlenecks

We analyze the energy bottlenecks in different systems. Fig. 5 shows the energy breakdown of representative memory-bound (MIS) and compute-bound (2mm) workloads. We make two key observations. First, compared to the 2D (3D) systems, the M3D-based system consumes on average 4.32 \times (4.76 \times) and 4.13 \times (3.32 \times) lower energy on compute-bound and memory-bound workloads, respectively. Second, even though for the memory-bound workloads, the main memory consumes a significant percentage of the overall energy in 2D and 3D, the main memory in the M3D baseline contributes to only 12% of total energy, turning the processor core into the most prominent contributor to the total energy consumption of the M3D baseline.

The energy benefits of the M3D baseline are due to two key factors. The first factor is related to the device-level advances in logic and memory layers, which, in fact, are orthogonal to the M3D integration. For example, the CNFET-based memory access circuits consume less power compared to MOSFETs [2], and the

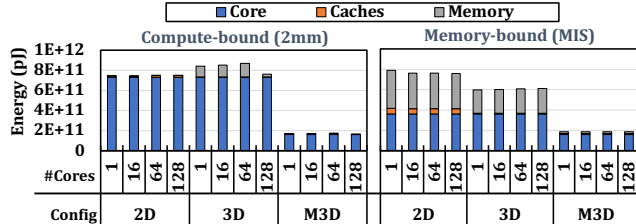


Fig. 5: Energy comparison.

⁵We do not change load/store queues or caches in this case.

deployed RRAM-based memory layers are more energy-efficient than DRAM [7–9]. The second factor is related to the M3D integration. As discussed in §2, M3D integration efficiently supports many memory channels, each connected to smaller memory arrays. Due to the shorter wire lengths within the memory arrays and the shorter global wires connecting the memory layers to logic layers on the same chip, the overall energy of memory accesses gets lowered with M3D integration.

4.3 Our Goal

Given the opportunities provided by M3D integration to drastically shift the performance and energy bottlenecks, it is important to understand the implications of this new technology on processor core and cache hierarchy designs that have been conventionally specialized to tackle main memory bottlenecks. **Our goal** in this work is to design the core and cache hierarchy, given the new trade-offs of M3D. While we focus on architecting M3D-based systems in this work, we argue that if other integration technologies (e.g., TSV-based or hybrid bonding) in the future achieve the same properties (e.g., pitch sizes) as current M3D integration technologies, our architectural insights can also be applied to systems built with such integration technologies.

5 Architecting the Processor Components

To design general-purpose processors based on the new opportunities and shifted bottlenecks of M3D-based systems, we analyze the design trade-offs of the cache hierarchy (§5.1) and cores (§5.2) in M3D. Table 4 summarizes (i) the key structures analyzed in this work, in different stages of an out-of-order superscalar processor core pipeline, (ii) the key analyzed aspect of each structure, and (iii) a pointer to the relevant sections.

Table 4: Analyzed pipeline elements.

Stage	Key Structure	Analyzed Aspect	Ptr.
Fetch	Instruction cache Branch predictor	Part of frontend bottleneck	§5.2.3
		Speculation bottleneck	§5.2.3
		Part of pipeline width	§5.2.1
Decode	Pre-decoder Decoder	Part of frontend bottleneck	§5.2.3
		Part of pipeline width	§5.2.1
Issue	Instruction window Reorder buffer	Part of pipeline width	§5.2.1
		Reorder buffer size	§5.2.2
Execution	Functional units	Part of pipeline width	§5.2.1
		Latency of micro-operations	§5.2.5
Memory	L1/L2 data caches	Cache size, latency, depth	§5.1
	Load/store queues	Load/store queue sizes	§5.2.2
	Threads communication	Synchronization	§5.2.4
Writeback	Register file (RF)	Part of pipeline width	§5.2.1

5.1 Cache Hierarchy

The design space of the cache hierarchy in M3D-based systems is affected by two conflicting factors. On one hand, M3D integration enables reducing the latency of caches through efficient 3D layouts (e.g., [53–56]) that reduce wire lengths. On the other hand, as discussed in §2, M3D integration enables improving main memory performance (bandwidth and latency), which reduces the impact of caches on the application performance. We evaluate the impact

of these conflicting factors on the performance of a wide range of workloads running on the M3D-based system.

5.1.1 Depth of the Cache Hierarchy. We compare noL2, an M3D-based system with no L2 cache⁶, and w/L2, an M3D-based system with a shared L2 cache. Fig. 6 shows the performance of a representative workload with low LFMR (atax) alongside the Average Memory Access Time (AMAT) and cache miss rates for a 64-core system. We make three observations. First, despite having a low L2 cache miss rate of 19% in w/L2 and a faster L2 compared to the M3D main memory, removing the L2 cache does not hurt performance.⁷ Second, we observe that the AMAT in noL2 is on par (even 4% lower) with the AMAT in w/L2. While removing the L2 cache does not significantly hurt AMAT for workloads with high L2 hit rates in M3D, removing it in the 3D baseline can lead to an up to 17× larger AMAT due to its slower main memory.

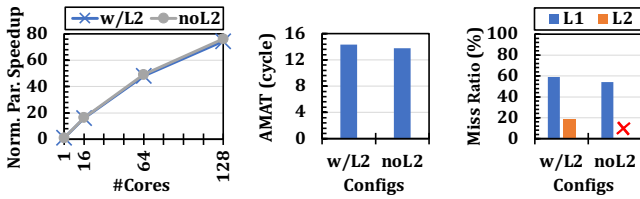


Fig. 6: Effect of no L2 cache on a low LFMR workload (atax).

Fig. 7 shows the performance, AMAT, and cache miss rates of a representative workload with high LFMR (MIS) for the same configurations. Based on this figure, we make three observations. First, noL2 improves performance by 17.8% on average across all core counts compared to both configurations with L2. Second, the L2 cache is highly ineffective (99% misses) in filtering accesses to the main memory. Third, the AMAT in noL2 is significantly lower than the two other configurations since it does not add extra L2 access latency and contention overhead. We conclude that removing the shared last-level L2 cache does not hurt performance for both classes of workloads. In fact, removing L2 leads to even a 10% average speedup across *all evaluated workloads*, with no workload experiencing a slowdown. Specifically, for bandwidth-bound workloads, removing L2 even increases performance scalability due to reduced cache contention. We observe 8%/8%/12%/18% average speedups for 1/16/64/128-core configurations.

Due to the importance of analyzing the impact of M3D architectural design decisions on an M3D-based system with different

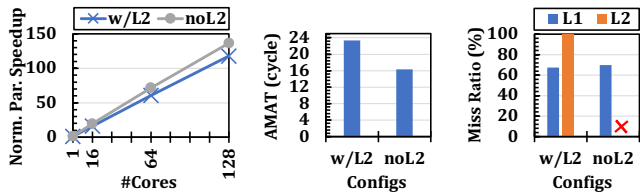


Fig. 7: Effect of no L2 cache on a high LFMR workload (MIS).

⁶Coherency is still maintained using a shared directory.

⁷Prior work (e.g., [104, 105]) has shown that removing shared caches can be effective for workloads with high cache miss rates, but it can degrade performance for workloads with strong cache locality [105]. In contrast, our results demonstrate that the improved main memory performance in M3D enables removing shared caches without negatively affecting *either class of workloads*.

latency values (as discussed in §3), we demonstrate the impact of cache hierarchy for an M3D-based system with different memory latency values. We keep the memory bandwidth the same (as listed in Table 3) across different configurations. Fig. 8 shows the performance of a low-LFMR workload (atax) on an M3D-based system with 64 processor cores in two different cases: (i) a configuration with no L2 (noL2), and (ii) a configuration with no L2, and where the area originally dedicated to L2 is used to increase the processor core's pipeline width (Wide+noL2), as extensively explained in §5.2.1 and §6. For each latency value, performance is normalized to the M3D baseline (with L2 cache and baseline pipeline width) with that latency value. We observe that even until 4× larger latency values, it is beneficial to use the logic area for increasing processing capability (e.g., wider pipeline) instead of larger caches. This is because the large M3D main memory bandwidth enables serving a larger number of in-flight requests. However, for larger latency values, having larger caches becomes critical.⁸

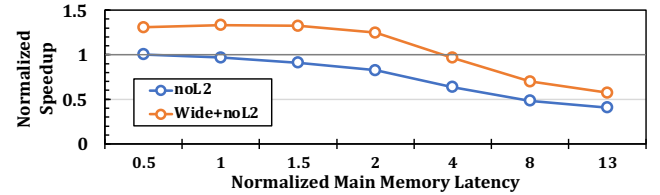


Fig. 8: Performance impact of removing the L2 cache on M3D-based systems with different memory latency values.

Lifetime Implications. While removing the shared caches increases the number of accesses to the main memory, the provisions for lifetime guarantees in the M3D baseline are already sufficient also for this case. This is because the baseline should already be designed for the worst-case scenario where the caches are not effective in filtering the main memory accesses (a common scenario for many memory-bound workloads). We observed that removing L2 does *not* change the overall number of accesses in many memory-bound workloads. Although removing shared caches increases the number of memory accesses in compute-bound workloads, these workloads have fewer total accesses compared to memory-bound workloads. Therefore, the baseline lifetime provisions are already sufficient.

5.1.2 Impact of Cache Size. We analyze the performance implication of increasing the L2 cache size. M3D facilitates circuit-level and device-level optimizations to increase cache size or reduce cache latency by designing vertical layouts of SRAM arrays to reduce the overall wire lengths. Analyzing the effects of such optimizations on M3D-based systems with logic and memory layers enables us to decide whether removing L2 in such systems is ultimately better than optimizing it. We analyze the performance of workloads with low and high LFRM, with varying L2 sizes and no L2. Even though increasing cache size can increase latency, we optimistically consider the ideal case where the latency does not increase with the cache size. Fig. 9 shows performance for representative workloads with high LFMR (PageRank) and low LFMR (2mm). We make three observations. First, larger caches improve the

⁸In §7, we analyze the impact of all RevaMp3D's design decisions in M3D-based systems with different latency values across all our workloads.

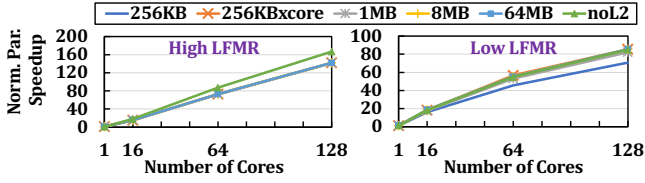


Fig. 9: Performance impact of L2 size.

performance of the low-LFMR workload by up to 22.7% compared to 256KB. Second, despite the benefits of larger L2 for low-LFMR workloads and the hit rate of up to 99% for the 64MB configuration, the performance of noL2 is similar to the performance with a larger L2 (64MB outperforms noL2 only by 3%), while incurring significantly less area overhead. Third, increasing the cache size does *not* improve performance for high-LFMR workloads since it does not reduce the cache miss rates. Across *all evaluated workloads* with different core counts, increasing the cache size leads to only a 3.7% average speedup. We conclude that a larger L2 does not lead to significantly better performance compared to *removing* it.

5.1.3 Impact of Cache Latency. We study the effect of reducing the latency of L1 and L2 caches. We analyze M3D-based system configurations where (i) the L1 latency is improved by 2 \times (L1fast), and (ii) the L2 latency is improved by 2 \times , and the L2 size is 64MB (L2Opt). Fig. 10 shows the performance effect of the mentioned cache configurations on representative workloads with high LFMR (MIS) and low LFMR (3mm). We make three observations. First, L2Opt improves performance by 5% compared to base for the high-LFMR workload, while removing the L2 cache outperforms the L2Opt case by 11% due to the high L2 miss rate of 99% in L2Opt. Second, even for the low-LFMR workload, we do not observe significant benefits in L2Opt compared to noL2. Third, for the high- and low-LFMR workloads, improving the L1 cache access latency leads to 5% and 10% performance improvements compared to base for high- and low-LFMR workloads, respectively. This is because L1 cache latency represents a large portion of the AMAT in M3D due to M3D’s fast main memory. Overall, we observe 12.5%/6% average speedup due to L1/L2 latency reduction across *all evaluated workloads*. We conclude that removing the shared L2 cache leads to better or comparable performance compared to larger or faster L2 caches. However, it is still important to reduce L1 latency.

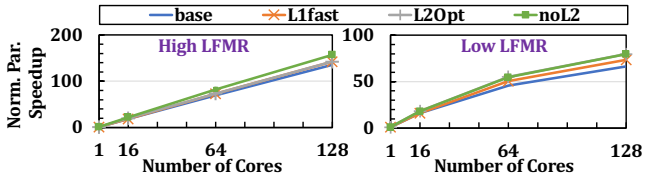


Fig. 10: Performance impact of cache latency.

5.2 Processor Core Design

5.2.1 Impact of Pipeline Width. We aim to understand the impact of wider pipelines in the M3D-based system in comparison to the 2D and 3D systems. Wider pipelines lead to a higher number of in-flight requests, which can be beneficial when the main memory can serve requests efficiently. Fig. 11 compares the speedup in 2D, 3D, and M3D-based systems when doubling the pipeline width for a

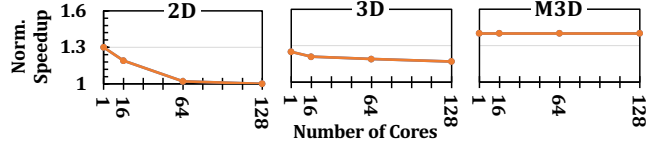


Fig. 11: Speedup of the wide pipeline for 2D, 3D, and M3D.

bandwidth-bound workload (BFS). Each data point is the speedup of each configuration after widening the pipeline over *the same configuration*. We observe that doubling the pipeline width provides a 40% speedup in the M3D-based system, while providing a lower speedup in the 2D and 3D systems. This is because, with large core counts, main memory bandwidth becomes a major performance bottleneck in the 2D and 3D systems and cannot service a higher number of requests from the wide pipeline. In the M3D-based system, across *all evaluated workloads*, we observe a 16% average speedup across all core counts. For compute-bound workloads with higher ILP, we observe an on-average 28% speedup. We conclude that wider pipelines provide relatively higher benefits to the M3D-based system compared to the 2D and 3D systems. We also analyze the effects of increasing the widths of different pipeline stages separately to understand whether significant benefits are obtained at lower area costs. We observe that doubling the width of *both* the backend and frontend leads to at least 1.27 \times higher average speedup than doubling the widths individually. As discussed in §5.1.1, Fig. 8 shows the performance of a wider pipeline on M3D-based systems with high memory bandwidth but varying memory latency values.

5.2.2 Size of Reordering Structures and Queues. We analyze the performance of the wide pipeline with (i) baseline load/store queues (L/SQ), issue queue, and reorder buffer (ROB) depths and (ii) two times deeper queues. We make three observations. First, larger queue sizes have a lower performance impact on the M3D-based system compared to the 3D system (12% in M3D versus 25% in 3D, across all evaluated workloads) due to lower instruction wait times in the M3D-based system. Second, despite the relatively lower impact of queue sizes in the M3D-based system, some workloads still take significant advantage of the larger queues (e.g., up to 20%). Third, increasing the issue queue’s depth increases the number of cycles spent in the issue stage, which can negatively impact the performance of *speculation-bound* workloads. Our analysis shows up to a 9.4% slowdown (for the speculation-bound workload, Triangle) due to the larger pipeline fill time and pipeline bubbles on branch mispredictions. However, as we show in §6.2, we can use the M3D-based system’s main memory to reduce this overhead for speculation-bound workloads.

5.2.3 Impact of Pipeline Frontend and Branch Prediction Units. Due to the increased impact of the frontend and speculation bottlenecks in M3D, we further study their implications on performance. For a representative speculation-bound workload (Triangle), Fig. 12 shows the performance of the baseline M3D-based system (Base) compared to M3D-based systems with (i) a state-of-the-art branch predictor [100] (TAGE-SC-L), (ii) an idealized frontend where the issue and dispatch structures in the pipeline take only one cycle (Shallow, i.e., a shallow pipeline that reduces the number of pipeline bubbles and fill latency in the event of branch misprediction), and (iii) an *idealized* branch prediction scheme, which leads to zero branch misprediction (Ideal-spec).

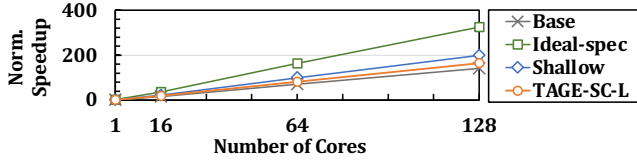


Fig. 12: Effect of speculation and frontend overheads.

We make two observations. First, while Ideal-spec leads to a 2.3 \times speedup compared to the baseline M3D-based system, using TAGE-SC-L [100] provides only a 14% speedup. This is due to the large number of hard-to-predict branches in this workload. Second, by reducing the overhead of branch misprediction, Shallow leads to up to 41% speedup for the speculation-bound workload. We conclude that improving the core’s frontend can lead to significant performance benefits (on average 15% across *all evaluated workloads*) by lowering the overhead of branch misprediction. §6.2 shows how RevaMp3D leverages the high-bandwidth M3D main memory to alleviate the misprediction overhead and frontend bottlenecks in the M3D-based systems with varying memory latency values.

5.2.4 Inter-Thread Communication. The large bandwidth of the M3D main memory can enable efficient feeding of data to a large number of threads. To take advantage of this high bandwidth, it is crucial to support efficient inter-thread communication. Fig. 13 shows the speedup of four microbenchmarks [106, 107], representing four commonly-used synchronization primitives in multi-threaded applications. We show the speedup of an M3D configuration where no overhead due to cache and memory latency is incurred during synchronization (Opt-sync),⁹ over an M3D configuration with baseline coherence-based synchronization (Base-sync). We observe on average 1.88 \times and up to 2.51 \times speedup and conclude that reducing synchronization overhead can provide significant performance benefits in M3D.

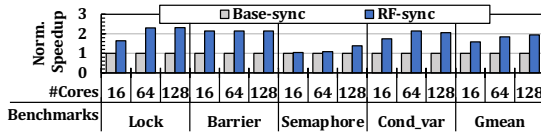


Fig. 13: Speedup of the optimized synchronization for different synchronization primitives.

We analyze the performance impact of synchronization overhead on M3D-based systems with large main memory bandwidth but with varying main memory latency values. Fig. 14 shows the speedup of an M3D configuration where no overhead due to cache and memory latency is incurred when performing synchronization

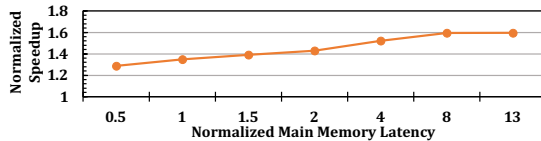


Fig. 14: Speedup of the optimized synchronization on M3D-based systems with different memory latency values.

⁹We consider horizontal wire delay (which also exists in the baseline) and only reduce the overhead of accessing the cache and main memory for synchronization variables.

over an M3D configuration with baseline coherence-based synchronization for a synchronization-heavy workload, Radix. We observe that the synchronization overhead increases on M3D-based systems with larger memory latency values.

5.2.5 Latency of Non-Memory Micro-Operations. We model an M3D-based system where *all* μ ops take one cycle and observe only a 5.4% average speedup compared to the M3D baseline for compute-bound workloads since most functional units are pipelined. We conclude that lowering the μ ops latency does not lead to significant speedup in M3D.

While in this work, we focus on the general-purpose processor cores and caches, §8 briefly discusses the new opportunities of M3D for other parts of the system stack and for domain-specific systems.

6 RevaMp3D: Architecting Processor Core and Cache Hierarchy Based on Implications of M3D Integration

We present RevaMp3D, an optimized M3D-based system, based on the implications of M3D integration on cache hierarchy and processor core design. We target performance bottlenecks in the M3D-based system and take advantage of opportunities offered by the M3D integration technology. Fig. 15 shows an overview of the key design decisions in RevaMp3D. §6.1 describes how RevaMp3D leverages the tight connectivity between M3D logic layers and §6.2 shows how RevaMp3D leverages M3D main memory to realize these design decisions.

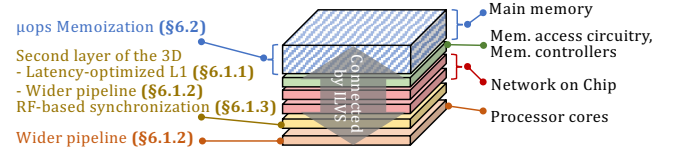


Fig. 15: Overview of the key design decisions in RevaMp3D.

6.1 Leveraging M3D Logic Layers

6.1.1 Cache Hierarchy. As described in §5.1, even an optimized L2 cache (with increased size or reduced latency) does not significantly outperform the configuration with no L2 cache. Hence, we remove the L2 cache from the cache hierarchy in RevaMp3D, which leads to freeing up 32% of the logic area. We then use this freed-up area for optimizations that alleviate the core bottlenecks and to widen and scale up various structures in the processor pipeline that enable greater instruction-level parallelism (§6.1.2). As described in §5.1, improving the L1 cache latency improves M3D performance due to the small AMAT in the M3D-based system. The short ILVs of the M3D integration technology enable efficient division of the SRAM structures between two logic layers to reduce the overall wire lengths in the SRAM structures, leading to reduced latency [14, 53–55]. Therefore, we leverage an M3D layout [14], which reduces L1 cache latency and planar footprint by 41% and 44%, respectively.

6.1.2 Pipeline Width. To design wider pipelines, first, we increase the width and depth of the pipeline SRAM structures (e.g., L/SQ, ROB), leading to an 11.6% area overhead per core (7.8% of the logic area). By exploiting the multi-layer SRAM structure supported by M3D [14, 54], we increase the size of these structures without increasing their latency and affecting the pipeline frequency. Second,

we increase the width of the decode structure and the functional units. Doubling the number of decode structures and functional units (including six integer ALUs, one FPU, and one complex ALU) leads to a 16.5% area overhead *per core* (11.2% of the logic area).¹⁰ We exploit part of the extra die area freed up due to removing the L2 cache to double the number of decode and execution units.

6.1.3 Register File-Level Synchronization. To facilitate high thread-level parallelism, we introduce a new fine-grained synchronization technique, using M3D technology’s dense inter-layer connectivity, to improve inter-thread communication. We use the thin inter-layer connections between the logic layers in the M3D system to perform fine-grained inter-thread communication in the register file (RF), instead of the memory hierarchy. The thin ILVs enable increasing the bandwidth of the SRAM cells in the RF by adding extra access transistors to each cell. The short ILVs can efficiently connect the extra access transistors in a secondary logic layer to the SRAM cells located on the primary layer, without increasing the RF latency. RevaMp3D leverages this to add extra ports to the RF of each core and uses the extra ports for fine-grained inter-thread communication. Fig. 16 shows how fine-grained ILVs can add additional access ports to an SRAM cell to increase bandwidth. *Small diameter* and *vertical* connections are essential for adding extra ports efficiently. Due to the small ILV diameter, such a vertical port layout increases the SRAM cell area at the 15nm technology node by less than 0.1%. However, for vertical connections with larger diameters (e.g., 2.6 μ m TSVs), this overhead increases significantly. For horizontal connections (i.e., in 2D), adding extra ports leads to not only area overhead, but also an increased lateral delay for accessing the port.

Due to RF’s limited size, we only leverage it for communications that involve small data, such as synchronization. While RF-level communication has been proposed in prior work [109], the adoption of such proposals is challenging in 2D or 3D systems due to the limitations of adding extra ports to the RFs. Without adding extra ports, the synchronization operations need to compete with the pipeline’s register operand accesses for the limited RF ports.

To enable fine-grained locking, where one lock variable is associated with a small amount of application data, each core writes the address of the data that is being locked by the core to other cores’ RF (instead of using lock variables updated through the cache hierarchy and the coherence protocol). Fig. 17 shows the speedup of RF

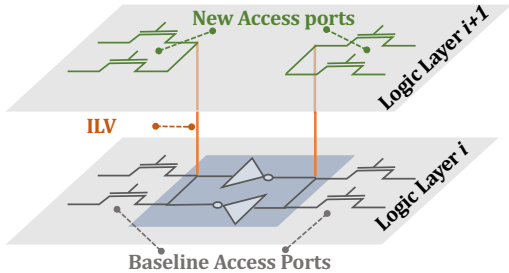


Fig. 16: Vertical layout to increase ports and bandwidth.

¹⁰We use McPAT [108] in 22nm technology for area analysis. Even though the absolute area values of the logic components in our CNFET-based M3D baseline do not equal the values generated by McPAT, we are interested in the area *ratio* of different logic components.

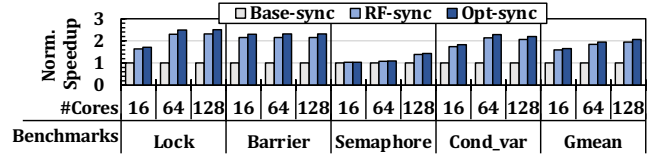


Fig. 17: Speedup of the register file-level synchronization.

synchronization (RF-sync) compared to the baseline (Base-sync) for the synchronization microbenchmarks. We observe on average 1.78 \times and up to 2.31 \times speedup over the M3D-based system with the baseline coherence-based synchronization.

Area and Timing Implications. In fine-grained locking schemes of real workloads, prior works [106, 110] show that the number of synchronization variables that are active at any given time during the execution is small (typically up to 4 variables). Thus, there is no need for large additional space in the RF. RF takes 0.2% of the logic area in our baseline. Therefore, the planar area overhead of adding extra ports to 4 entries of the RF is less than 0.001% of the logic area. Since the extra ports are connected to RF entries from another logic layer using the short ILVs, they do not change the structure and timing of the RF accesses for the baseline core operations.

Security Implications. This technique does not exacerbate the security guarantees compared to the baseline system due to two reasons. First, we propose this technique for threads that are from the same multi-threaded application (with a similar protection domain and from one user). Therefore, threads from different applications, users, or protection domains do not access each other’s data in the register file for synchronization. Second, threads spawned from one application already exchange data through the cache coherence protocol, which has already led to multiple attacks that leverage the coherence traffic to establish side channels. We conclude that utilizing the register file for synchronization does not open up new attack surfaces and does not exacerbate the existing security issues with data coherence.

6.2 Leveraging M3D Memory Layers

We propose a new processor frontend design that memoizes the repetitive fetched, decoded, and re-ordered μ ops, stores them in M3D main memory, and turns off the relevant parts of the core pipeline when the same μ ops execute in a loop. The high-bandwidth, energy-efficient M3D memory enables storing and loading the memoized instructions efficiently. This addresses two key bottlenecks that we identify in the M3D baseline. First, it can alleviate the shifted M3D system’s energy bottlenecks that are dominated by the processor core’s energy consumption. As programmers commonly use loops in their codes, a significant number of instructions in programs are typically repeated [64, 65, 111]. Therefore, turning off the frontend and reordering structures can lead to energy saving by eliminating a significant portion of the average energy per core in the baseline OoO core. Second, this technique alleviates the speculation bottleneck in the M3D system by reducing the pipeline fill latency and number of pipeline bubbles in the event of branch misprediction since the instructions do not need to be fetched, decoded, and reordered if they are already memoized.

While prior works [64, 111] have also explored μ op memorization with an Execution Cache (EC), these works leverage SRAM-based

caches that incur large area overheads. However, RevaMp3D leverages the high-bandwidth connection between logic and memory layers as a unique opportunity provided by the M3D integration technology, and stores the memorized μ ops in the main memory. Prior work [64] shows that to fully benefit from the μ op memoization technique, we need a large on-chip EC (e.g., up to 100KB) per core, which incurs high area overheads, occupying 15% of the logic area of the baseline processor core. Considering a fixed area budget, this overhead can come at the cost of key core components and, therefore, sacrifice performance. Some prior works propose a smaller EC for area efficiency but at the cost of memoizability opportunities in applications with a large instruction footprint and large loops [64, 111–113]. In contrast, using M3D main memory for storing the memorized μ ops paves the way for architecting a large and scalable EC at low area cost. We use a small buffer to store the prefetched memoized μ ops from main memory and provide a one-cycle access latency.

Fig. 18 demonstrates Energy per Instruction (EPI) in (1) no memoization (No-Memo), (2) memoizing μ ops in a 100KB-SRAM EC (Baseline-Memo), and (3) memoizing μ ops in M3D main memory (M3D-Memo). In (2) and (3), the frontend, decode, and reordering structures are power-gated when the memoized μ ops execute. We break down the EPI to the energy spent on the core, the SRAM-based EC (Cache-EC) in Baseline-Memo, and the main memory-based EC (M3D-EC) and the small buffer (Buffer-EC) in M3D-Memo. We observe that M3D-Memo reduces EPI by 37% over No-Memo and achieves comparable EPI compared to Baseline-Memo, while incurring significantly lower area cost.

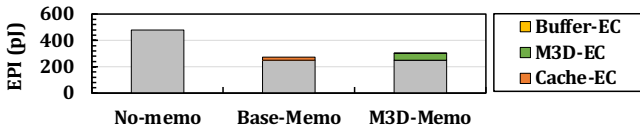


Fig. 18: Energy per instruction of three design points.

Implementation. We implement M3D-Memo based on prior work [64] that proposes an SRAM-based EC. As shown in Fig. 19, we place the *Memoization Unit (MU)* after the issue stage in the pipeline. Note that the MU does not add an extra stage to the pipeline since instructions are issued to the execution stage and the MU in parallel. We use the high main memory bandwidth in M3D to memoize both the taken and not-taken paths of hard-to-predict branches. The MU has three main components: ① a small 1.28KB SRAM buffer to provide one-cycle access latency to the memoized μ ops, ② a simple stride prefetcher that reads μ ops from the main memory and fills the buffer to hide the memory access latency, and ③ a memory interface that uses two read/write ports for the taken and not-taken paths and an address bus. We calculate the area of the MU unit using Synopsys Design Compiler and show that it occupies less

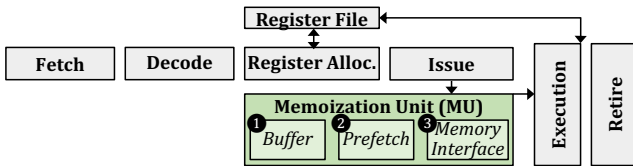


Fig. 19: RevaMp3D's Memoization Unit.

than 5% of the L1 cache area. We use a preserved address space to store the memoized μ ops. As we are not limited in capacity, we can capture up to 100% of the memoizable μ ops.

Performance Implications. M3D-Memo improves the performance of speculation-bound workloads by reducing pipeline fill latency and bubbles. However, M3D-Memo *limits* renaming each architectural register to a specific register pool (similar to [64]), which can negatively affect performance. Overall, the effect of reducing pipeline depth and fill latency in the M3D-based system outweighs this overhead, leading to up to 35.5% speedup for speculation-bound workloads and a modest average speedup of 1.4% across all evaluated workloads.

To demonstrate the impact of this design as the M3D memory latency changes, Fig. 20 shows the performance of a 64-core M3D-based system with the main memory-based μ op memorization technique for a speculation-bound workload (Tri). Performance at each point is normalized against the baseline M3D-based system with that memory latency value. In all configurations, the M3D-based system has the same bandwidth. We find that the main memory-based μ op memoization technique achieves significant speedups (22–42%) across a range of memory latencies, with particularly larger gains at lower latency values.

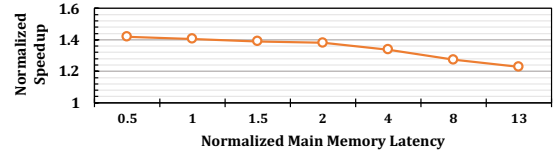


Fig. 20: Performance impact of the μ op memoization technique on M3D-based systems with different memory latency values.

7 End-to-End Evaluation

7.1 End-to-End Speedup

Fig. 21 (a) shows the speedup of RevaMp3D (with all design decisions of §6) over the state-of-the-art M3D system, across all multi-threaded workloads and the multi-programmed workload mixes. Each data point shows the speedup of the optimized M3D with N cores over the baseline M3D with N cores, where $N \in \{1, 16, 64, 128\}$. We make two observations. First, we observe a significant performance improvement, on average 80.6% and 67.6% speedups across all core counts for multi-threaded workloads and multi-programmed workload mixes, respectively. Second, the suggested design decisions improve the performance of *all evaluated workloads* (i.e., no workload suffers from slowdown).

Fig. 21 (b) shows RevaMp3D's speedup, averaged across all evaluated workloads, over the state-of-the-art 2D, 3D, and M3D-based systems. We observe that RevaMp3D provides significant benefits, resulting in 7.14 \times and 4.96 \times speedups over the 2D and 3D systems, respectively, further increasing the potential performance benefits of M3D integration.

For varying main memory latency values, Fig. 22 shows the distribution of the end-to-end speedup of RevaMp3D over the baseline M3D-based system across all the workloads. RevaMp3D's speedup at each memory latency point is reported relative to the performance of the baseline system at that same latency. Both RevaMp3D

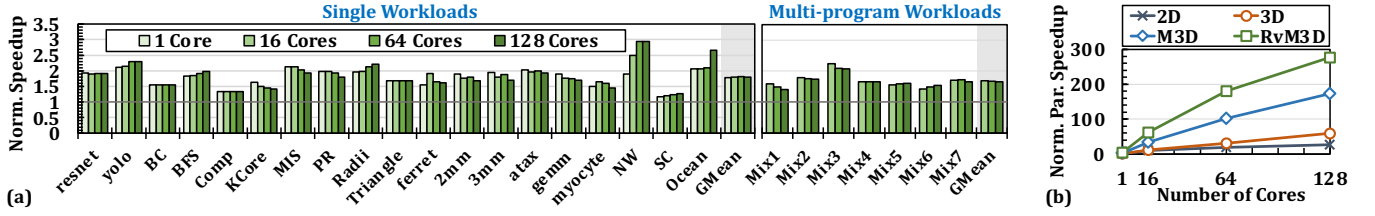


Fig. 21: RevaMp3D's Speedup over (a) the M3D baseline, and (b) the 2D and 3D baselines on average across all evaluated workloads.

and baseline feature 64 cores. We observe that RevaMp3D provides speedup for all evaluated workloads even when memory latency increases to $2\times$ larger, while some workloads exhibit slowdowns at higher latencies. This is because, as shown in Fig. 8, some design decisions in RevaMp3D are primarily tailored for smaller latency values. While not all RevaMp3D design choices lead to speedup for M3D-based systems with high latency, the high-bandwidth connectivity between logic and memory layers in the M3D-based system can still provide several benefits (e.g., RF-based inter-thread synchronization and the efficient μ op memorization), which provide benefits for M3D-based systems different memory latency values. Therefore, depending on the configuration of the M3D-based system and its main memory characteristics, different subsets of RevaMp3D's design decisions can be adopted to enhance both performance and energy efficiency.

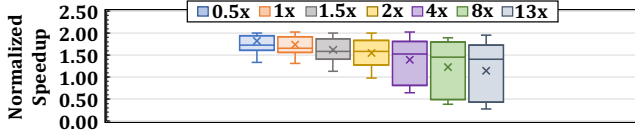


Fig. 22: RevaMp3D's speedup with various memory latencies.

7.2 Analysis of Different RevaMp3D Configurations

We evaluate the benefits of four different RevaMp3D configurations, each optimized for different goals. Fig. 23 shows the normalized speedup and energy consumption of each configuration relative to the baseline M3D-based system, averaged across all evaluated workloads. First, RvM3D-P represents the RevaMp3D configuration that only applies the performance-improving design decisions in §6.1. Second, RvM3D-E represents the configuration that only applies the design decisions in §6.2, with the main goal of reducing energy consumption. Third, RvM3D represents a configuration that combines both sets of design decisions. Fourth, RvM3D-I represents a low-frequency implementation of RevaMp3D that is iso-power with the M3D baseline. We make four observations.

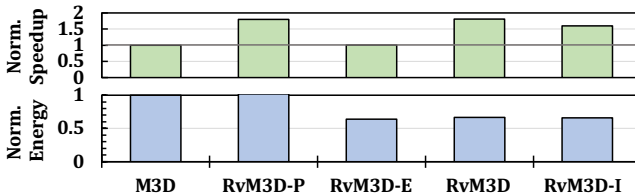


Fig. 23: Speedup and energy of RevaMp3D's configurations.

First, RvM3D-P leads to similar average energy consumption compared to the M3D baseline (with only a modest 2% increase). This is because, given the high energy efficiency of the M3D main memory, removing L2 does not lead to a significant increase in energy consumption. Furthermore, increasing the width of the pipeline SRAM structures using the M3D vertical layout [14] does not increase their energy per access since their overall planar wire length does not increase. Second, RvM3D-E leads to 36.6% lower average energy consumption since, for each of our workloads, we observe a high degree of memoizability, where at least 99% of their dynamic instructions follow the same schedule. RvM3D-E leads to an average speedup of 1.4%. Third, RvM3D leads to an on-average 80.6% speedup. While the performance-improving design decisions lead to an 84% power increase over the baseline M3D, the memoization technique allows this performance improvement at only 18% higher power consumption. Fourth, RvM3D-I outperforms the 4GHz baseline M3D by 60.5%, without an increase in power consumption. We conclude that our approach increases the M3D-based system's performance per Watt by both improving performance and lowering energy consumption.

7.3 Overall Area Reduction

We summarize the area impact of RevaMp3D in Table 5. We observe an *overall* 12.3% area reduction compared to the baseline M3D-based system. The freed-up area can be used to further improve performance (e.g., by adding more cores). RevaMp3D re-purposes the logic layer used for the L2 cache in the baseline M3D-based system (shown in Fig. 2) to add all the needed components (e.g., the extra RF ports, the second layer of the L1 cache, and the second layer of the wider pipeline's SRAM structures and its additional functional units), while consuming smaller logic area than the L2 cache.

Table 5: Area Impact of RevaMp3D.

Proposed Change	Area Impact (% of logic area)
L2 cache removal	-32%
Wider pipeline	+19%
EC Buffer	+0.7%
Register file overheads	< +0.01%
Total	-12.3%

8 Discussion

Scaling Data Size Beyond Main Memory Capacity. While a system with a single M3D chip can potentially provide hundreds of gigabytes of main memory [7, 9], for even larger requirements, a system can employ multiple M3D chips. In that case, off-chip access

costs more overhead than on-chip access, and techniques that alleviate the remote access overhead using scheduling, data placement, replication, or migration can be orthogonally applied [69, 114, 115]. Advances in integration technology can further reduce the cost of off-chip accesses in M3D by enabling the monolithic integration of multiple M3D stacks [116].

HW/SW Co-Design. Memory bottleneck affects both hardware and software in today’s systems. This work explores the implications of M3D on the hardware design of cores and caches. We believe that it is essential to also revisit the software stack to better leverage the underlying M3D hardware. In the operating systems, memory management and process management units can be revisited to be aware of M3D’s trade-offs. At the application level, it is critical to revisit the optimizations targeted toward addressing memory bottlenecks versus other bottlenecks. We hope our analysis of new bottlenecks and opportunities of M3D systems guides future software development for this technology.

Applicability to Domain-Specific Systems. While our work focuses on general-purpose systems, our observations and design trade-offs can also be considered when designing domain-specific systems. For example, we expect to observe bottleneck shifts as shown in our analysis. Based on the structure of the accelerator, the alleviated memory bottleneck can enable reducing the size of on-chip buffers, increasing the width or number of processing elements, and providing memoization opportunities. The tight connection between the layers can facilitate communication between different accelerator units in different logic layers in M3D. A detailed analysis of domain-specific M3D requires its own separate study based on the accelerator domain and is outside the scope of this work.

9 Related Work

To our knowledge, this is the first work to re-examine the processor core and cache hierarchy based on rigorous bottleneck analysis of a wide range of workloads and the new trade-offs imposed by M3D integration. We briefly discuss previous works in designing M3D-based systems.

Device and Circuit-Level Integration. Many works (e.g., [34–42, 117–124]) focus on the design of efficient M3D devices with respect to performance, power, energy, area, temperature, yield and reliability. Other studies show the benefits of M3D technology in comparison to 3D-stacked technologies [43, 44]. Several works (e.g., [3, 10, 45]) study M3D physical integration and layout. Several works explore heterogeneous device layers in M3D (e.g., [46–49, 125]).

Designing M3D Processors. Recent works propose 3D partitioning techniques for logic-only M3D processors (e.g., [14, 50, 51]) to improve the latency of different components by decreasing their wire lengths. Other works show how to leverage M3D to design efficient SRAMs (e.g., [53–56]) or NoCs (e.g., [50, 52]). Some works (e.g., [3, 52]) discuss the memory system challenges, such as optimizing the memory array structures and developing techniques to increase memory parallelism (e.g., SIMD units and non-blocking loads). Some works explore the benefits of M3D integration of non-volatile memory on top of last-level caches and how to design the interface between them (e.g., [3, 6, 10]). While prior works propose various optimizations, we analyze the implications of M3D on (i) the real-world application bottlenecks and (ii) architectural designs that

have been conventionally specialized to tackle the memory bottleneck. For example, while prior works propose optimizations to caches in M3D [9, 14], we show that such optimizations are *not essential* beyond L1 for M3D-based systems with low memory latency values.

Accelerating Specific Applications. Various works (e.g., [51, 57–63, 126–129]) design domain-specific accelerators in M3D. Some works (e.g., [130]) suggest M3D FPGAs. While our work focuses on general-purpose systems, §8 discusses how our design choices can also inspire domain-specific systems.

Processing-Using-Memory in M3D-based systems. Some works (e.g., [125, 131, 132]) design processing-using-memory systems specialized for M3D-integrated systems.

3D-Integrated Caches. Prior works propose 3D-integrated caches to achieve low latency and high bandwidth, such as AMD’s 3D SRAM V-Cache [133] and SILO [134]. However, due to their limited capacity, these solutions cannot fully address main memory bottlenecks.

10 Conclusion

In this work, we design the processor core and cache hierarchy, given the fundamentally new trade-offs of M3D integration technology. We show that for a variety of workloads on a state-of-the-art M3D-based system, the performance and energy bottlenecks substantially shift from the main memory to the processor core and cache hierarchy, emphasizing the need to revisit current designs. We conduct a rigorous design space exploration of the key components of the processor core and cache hierarchy to understand the implications of the M3D-based system’s shifted bottlenecks on their design. Based on these implications and by taking advantage of the new opportunities of M3D integration, we design a new M3D-based system, RevaMp3D. We show that RevaMp3D provides significant performance improvement and energy reduction while achieving a smaller logic area compared to the state-of-the-art M3D-based system.

References

- [1] T Srimani, A Bechdolt, S Choi, C Gilardi, A Kasperovich, S Li, Q Lin, M Malakoutian, P McEwen, RM Radway, et al. N3xt 3d technology foundations and their lab-to-fab: Omni 3d logic, logic+ memory ultra-dense 3d, 3d thermal scaffolding. In *2023 International Electron Devices Meeting (IEDM)*. IEEE, 2023.
- [2] Max M Shulaker, Gage Hills, Nishant Patil, Hai Wei, Hong-Yu Chen, H-S Philip Wong, and Subhasish Mitra. Carbon nanotube computer. *Nature*, 501(7468):526–530, 2013.
- [3] Candace Walden, Devesh Singh, Meenatchi Jagasivamani, Shang Li, Luyi Kang, Mehdi Asnaashari, Sylvain Dubois, Bruce Jacob, and Donald Yeung. Monolithically integrating non-volatile main memory over the last-level cache. *ACM Transactions on Architecture and Code Optimization (TACO)*, 2021.
- [4] Subir Ghosh, Yikai Zheng, Zhiyu Zhang, Yongwen Sun, Thomas F Schrammer, Najam U Sakib, Aaryan Oberoi, Chen Chen, Joan M Redwing, Yang Yang, et al. Monolithic and heterogeneous three-dimensional integration of two-dimensional materials with high-density vias. *Nature Electronics*, 2024.
- [5] Max M Shulaker, Tony F Wu, Asish Pal, Liang Zhao, Yoshio Nishi, Krishna Saraswat, H-S Philip Wong, and Subhasish Mitra. Monolithic 3D Integration of Logic and Memory: Carbon Nanotube FETs, Resistive RAM, and Silicon FETs. In *IEDM*, 2014.
- [6] Meenatchi Jagasivamani, Candace Walden, Devesh Singh, Luyi Kang, Mehdi Asnaashari, Sylvain Dubois, Bruce Jacob, and Donald Yeung. Tileable monolithic rram memory design. In *2020 IEEE Symposium in Low-Power and High-Speed Chips (COOL CHIPS)*. IEEE, 2020.
- [7] Max M Shulaker, Gage Hills, Rebecca S Park, Roger T Howe, Krishna Saraswat, H-S Philip Wong, and Subhasish Mitra. Three-dimensional integration of nanotechnologies for computing and data storage on a single chip. *Nature*, 547(7661):74–78, 2017.

- [8] Mohamed M Sabry Aly, Mingyu Gao, Gage Hills, Chi-Shuen Lee, Greg Pitner, Max M Shulaker, Tony F Wu, Mehdi Asheghi, Jeff Bokor, Franz Franchetti, Kenneth E Goodson, Christos Kozyrakis, Igor Markov, Kunle Olukotun, Larry Pileggi, Eric Pop, Jan Rabaey, Christopher Re, H.-S. Philip Wong, and Subhasish Mitra. Energy-efficient abundant-data computing: The n3xt 1,000 x. *Computer*, 48(12):24–33, 2015.
- [9] Mohamed M Sabry Aly, Tony F Wu, Andrew Bartolo, Yash H Malviya, William Hwang, Gage Hills, Igor Markov, Mary Wootters, Max M Shulaker, H-S Philip Wong, and Subhasish Mitra. The N3XT Approach to Energy-Efficient Abundant-Data Computing. *IEEE '18*.
- [10] Meenatchi Jagasivamani, Candace Walden, Devesh Singh, Luyi Kang, Shang Li, Mehdi Asnaashari, Sylvain Dubois, Bruce Jacob, and Donald Yeung. Analyzing the monolithic integration of a reraam-based main memory into a cpu's die. *IEEE Micro*, 2019.
- [11] Yuanqing Cheng, Xiaochen Guo, and Vasilis F Pavlidis. Emerging monolithic 3d integration: Opportunities and challenges from the computer system perspective. *Integration*, 85:97–107, 2022.
- [12] NVidia. NVIDIA A100 Tensor Core GPU Architecture, 2020. <https://www.nvidia.com/en-us/data-center/a100/>.
- [13] SK Hynix. Fastest DRAM with enhanced heat dissipation, 2021. <https://product.skhynix.com/products/dram/hbm/hbm2e.go>.
- [14] Bhargava Gopireddy and Josep Torrellas. Designing Vertical Processors in Monolithic 3D. In *ISCA*, 2019.
- [15] Soon-Wook Kim, Mikael Detalle, Lan Peng, Philip Nolmans, Nancy Heylen, Dimitrios Velenis, Andy Miller, Gerald Beyer, and Eric Beyne. Ultra-fine pitch 3d integration using face-to-face hybrid wafer bonding combined with a via-middle through-silicon-via process. In *2016 IEEE 66th Electronic Components and Technology Conference (ECTC)*, pages 1179–1185. IEEE, 2016.
- [16] Dimin Niu, Shuangchen Li, Yuhao Wang, Wei Han, Zhe Zhang, Yijin Guan, Tianchan Guan, Fei Sun, Fei Xue, Lide Duan, Yuanwei Fang, Hongzhong Zheng, Xiping Jiang, Song Wang, Fengguo Zuo, Yubing Wang, Bing Yu, Qiwei Ren, and Yuan Xie. 184qps/w 64mb/mm 2 3d logic-to-dram hybrid bonding with process-near-memory engine for recommendation system. In *ISSCC*, 2022.
- [17] Bai Fujun, Jiang Xiping, Wang Song, Yu Bing, Tan Jie, Zuo Fengguo, Wang Chunjuan, Wang Fan, Long Xiaodong, Yu Guoqing, Fu Ni, Li Qiannan, Li Hua, Wang Kexin, Duan Huifu, Bai Liang, Jia Xuerong, Li Jin, Li Mei, Wang Zhengwen, Hu Sheng, Zhou Jun, Zhan Qiong, Sun Peng, Yang Daohong, Cheichan Kau, David Yang, Ching-Sung Ho, Sun Hongbin, Lv Hangbing, Liu Ming, Kang Yi, and Ren Qiwei. A stacked embedded dram array for lpddr4/4x using hybrid bonding 3d integration with 34gb/s/1gb 0.88 pj/b logic-to-memory interface. In *2020 IEEE International Electron Devices Meeting (IEDM)*, pages 6–6. IEEE, 2020.
- [18] L. Arnaud, C. Karam, N. Bresson, C. Dubarry, M. Borel, M. Assous, G. Mauguen, F. Fournel, M. Gottardi, T. Mourier, S. Cheramy, and F. Servant. Three-dimensional hybrid bonding integration challenges and solutions toward multi-wafer stacking. *MRS communications*, 10(4):549–557, 2020.
- [19] Han-Wen Hu and Kuan-Neng Chen. Development of low temperature cucu bonding and hybrid bonding for three-dimensional integrated circuits (3d ic). *Microelectronics Reliability*, 127:114412, 2021.
- [20] Theodoros Nigussie, Tse-Han Pan, Steve Lipa, W Shepherd Pitts, Javi DeLaCruz, and Paul Franzon. Design benefits of hybrid bonding for 3d integration. In *2021 IEEE 71st Electronic Components and Technology Conference (ECTC)*, pages 1876–1881. IEEE, 2021.
- [21] Yiwei Du, Jianshi Tang, Yijun Li, Yue Xi, Yuankun Li, Jiaming Li, Heyi Huang, Qi Qin, Qingtian Zhang, Bin Gao, et al. Monolithic 3d integration of analog rram-based computing-in-memory and sensor for energy-efficient near-sensor computing. *Advanced Materials*, 2024.
- [22] Chanseul Lee, Sunbum Kim, Gyulee Kim, and Changhwan Choi. Heterogeneous monolithic 3d integration for hybrid vertical cmos inverter using n-type igto tft on p-type si fet. *Materials Science in Semiconductor Processing*, 185:108871, 2025.
- [23] Zhenyu Wang, Pragnya Sudershan Nalla, Jingbo Sun, A Alper Goksoy, Sumit K Mandal, Jae-sun Seo, Vidya A Chhabria, Jeff Zhang, Chaitali Chakrabarti, Umith Ogras, et al. Hisim: Analytical performance modeling and design space exploration of 2.5 d/3d integration for ai computing. *IEEE Transactions on Computer-Aided Design of Integrated Circuits and Systems*, 2025.
- [24] Ali Sedaghatgoo, Amir M Hajisadeghi, Mahmoud Momtazpour, and Nader Bagherzadeh. Arman: A reconfigurable monolithic 3d accelerator architecture for convolutional neural networks. *arXiv preprint arXiv:2402.04431*, 2024.
- [25] Kyungwook Chang and Sung Kyu Lim. Design and tool solutions for monolithic three-dimensional integrated circuits. In *Handbook of Computer Architecture*. Springer, 2024.
- [26] Sai Pentapati and Sung-Kyu Lim. Heterogeneous monolithic 3-d ic designs: Challenges, eda solutions, and power, performance, cost tradeoffs. *IEEE Transactions on Very Large Scale Integration (VLSI) Systems*, 2024.
- [27] Jinwoo Kim, Lingjun Zhu, Hakki Mert Torun, Madhavan Swaminathan, and Sung Kyu Lim. A ppa study for heterogeneous 3-d ic options: Monolithic, hybrid bonding, and microbumping. *IEEE Transactions on Very Large Scale Integration (VLSI) Systems*, 32(3):401–412, 2023.
- [28] SkyWater. SkyWater Technology Foundry Selects Veeco's Waferstorm for 3D Monolithic System-on-a-Chip Development. <https://www.skywatertechnology.com/skywater-technology-foundry-selects-veeco-waferstorm-for-3d-monolithic-system-on-a-chip-development/>.
- [29] S Liao, L Yang, TK Chiu, WX You, TY Wu, KF Yang, WY Woon, WD Ho, ZC Lin, HY Hung, et al. Complementary field-effect transistor (cfet) demonstration at 48nm gate pitch for future logic technology scaling. In *2023 International Electron Devices Meeting (IEDM)*, pages 1–4. IEEE, 2023.
- [30] S Subramanian, M Hosseini, T Chiarella, S Sarkar, P Schuddinck, BT Chan, D Radisic, G Mannaert, A Hikavy, E Rosseel, et al. First monolithic integration of 3d complementary fet (cfet) on 300mm wafers. In *2020 IEEE Symposium on VLSI Technology*, pages 1–2. IEEE, 2020.
- [31] Ki Seok Kim, Seunghwan Seo, Junyoung Kwon, Doyoon Lee, Changhyun Kim, Jung-El Ryu, Jekyung Kim, Jun Min Suh, Hang-Gyo Jung, Youhwan Jo, et al. Growth-based monolithic 3d integration of single-crystal 2d semiconductors. *Nature*, 636(8043):615–621, 2024.
- [32] S. Subramanian, M. Hosseini, T. Chiarella, S. Sarkar, P. Schuddinck, B. T. Chan, D. Radisic, G. Mannaert, A. Hikavy, E. Rosseel, F. Sebaai, A. Peter, T. Hopf, P. Morin, S. Wang, K. Devriendt, D. Batuk, G. T. Martinez, A. Veloso, E. Dentoni Litta, S. Baudot, Y. K. Siew, X. Zhou, B. Briggs, E. Capogreco, J. Hung, R. Koret, A. Spessot, J. Ryckaert, S. Demuynck, N. Horiguchi, and J. Boemmels. First monolithic integration of 3d complementary fet (cfet) on 300mm wafers. In *2020 IEEE Symposium on VLSI Technology*, 2020.
- [33] FF Athena, E Ambrosi, K Jana, CH Wu, J Hartanto, YM Lee, CC Kuo, S Liu, B Saini, CC Wang, et al. First demonstration of an np oxide semiconductor complementary gain cell memory. In *2024 IEEE International Electron Devices Meeting (IEDM)*, pages 1–4. IEEE, 2024.
- [34] Bon Woong Ku, Peter Debacker, Dragomir Milojevic, Praveen Raghavan, Diederik Verkest, Aaron Thean, and Sung Kyu Lim. Physical design solutions to tackle feol/beol degradation in gate-level monolithic 3d ics. In *Proceedings of the 2016 International Symposium on Low Power Electronics and Design*, pages 76–81, 2016.
- [35] Chang Liu and Sung Kyu Lim. A design tradeoff study with monolithic 3d integration. In *Thirteenth International Symposium on Quality Electronic Design (ISQED)*, pages 529–536. IEEE, 2012.
- [36] Shreepad Panth, Sandeep Samal, Yun Seop Yu, and Sung Kyu Lim. Design challenges and solutions for ultra-high-density monolithic 3d ics. In *2014 SOI-3D-Subthreshold Microelectronics Technology Unified Conference (S3S)*, pages 1–2. IEEE, 2014.
- [37] Kyungwook Chang, Abhishek Koneru, Krishnendu Chakrabarty, and Sung Kyu Lim. Design automation and testing of monolithic 3d ics: Opportunities, challenges, and solutions. In *2017 IEEE/ACM International Conference on Computer-Aided Design (ICCAD)*, 2017.
- [38] Sandeep Kumar Samal, Shreepad Panth, Kambiz Samadi, Mehdi Saedi, Yang Du, and Sung Kyu Lim. Fast and Accurate Thermal Modeling and Optimization for Monolithic 3D ICs. In *DAC '14*.
- [39] Prachi Shukla, Ayse K Coskun, Vasilis F Pavlidis, and Emre Salman. An overview of thermal challenges and opportunities for monolithic 3d ics. In *Proceedings of the 2019 on Great Lakes Symposium on VLSI*, pages 439–444, 2019.
- [40] Dongjin Lee, Sourav Das, Janardhan Rao Doppa, Partha Pratim Pande, and Krishnendu Chakrabarty. Performance and thermal tradeoffs for energy-efficient monolithic 3d network-on-chip. *ACM Transactions on Design Automation of Electronic Systems (TODAES)*, 23(5):1–25, 2018.
- [41] Sandeep Kumar Samal, Kambiz Samadi, Pratyush Kamal, Yang Du, and Sung Kyu Lim. Full chip impact study of power delivery network designs in monolithic 3d ics. In *2014 IEEE/ACM International Conference on Computer-Aided Design (ICCAD)*, pages 565–572. IEEE, 2014.
- [42] Melanie Brocard, Benoit Mathieu, Jean-Philippe Colonna, Cristiano Santos, Claire Fenouillet-Beranger, Vincent Lu Cao-Minh, Gerald Cibrario, Laurent Brunet, Perrine Batude, François Andrieu, Sebastian Thuries, and Olivier Billoint. Transistor temperature deviation analysis in monolithic 3d standard cells. In *2017 IEEE Computer Society Annual Symposium on VLSI (ISVLSI)*, pages 539–544. IEEE, 2017.
- [43] Sandeep Kumar Samal, Deepak Nayak, Motoi Ichihashi, Srinivasa Banna, and Sung Kyu Lim. Monolithic 3d ic vs. tsv-based 3d ic in 14nm finfet technology. In *2016 IEEE SOI-3D-Subthreshold Microelectronics Technology Unified Conference (S3S)*, pages 1–2. IEEE, 2016.
- [44] Deepak Kumar Nayak, Srinivasa Banna, Sandeep Kumar Samal, and Sung Kyu Lim. Power, performance, and cost comparisons of monolithic 3d ics and tsv-based 3d ics. In *2015 IEEE SOI-3D-Subthreshold Microelectronics Technology Unified Conference (S3S)*, pages 1–2. IEEE, 2015.
- [45] Meenatchi Jagasivamani, Candace Walden, Devesh Singh, Luyi Kang, Shang Li, Mehdi Asnaashari, Sylvain Dubois, Donald Yeung, and Bruce Jacob. Design for reraam-based main-memory architectures. In *Proceedings of the International Symposium on Memory Systems*, 2019.
- [46] Farzaneh Zokaee, Mingzhe Zhang, Xiaochun Ye, Dongrui Fan, and Lei Jiang. Magma: A monolithic 3d vertical heterogeneous reraam-based main memory architecture. In *2019 56th ACM/IEEE Design Automation Conference (DAC)*. IEEE,

2019.

- [47] Gauthaman Murali, Xiaoyu Sun, Shimeng Yu, and Sung Kyu Lim. Heterogeneous mixed-signal monolithic 3-d in-memory computing using resistive ram. *IEEE Transactions on Very Large Scale Integration (VLSI) Systems*, 2020.
- [48] Anwesha Chatterjee, Shouvik Musavvir, Ryan Gary Kim, Janardhan Rao Doppa, and Partha Pratim Pande. Power management of monolithic 3d manycore chips with inter-tier process variations. *ACM Journal on Emerging Technologies in Computing Systems (JETC)*, 2021.
- [49] Gauthaman Murali and Sung Kyu Lim. Heterogeneous 3d ics: Current status and future directions for physical design technologies. In *2021 Design, Automation & Test in Europe Conference & Exhibition (DATE)*, pages 146–151. IEEE, 2021.
- [50] Dylan Stow, Itir Akgun, Wenqin Huangfu, Yuan Xie, Xueqi Li, and Gabriel H Loh. Efficient System Architecture in the Era of Monolithic 3D: Dynamic Inter-tier Interconnect and Processing-in-Memory. In *DAC '19*, 2019.
- [51] Biresh Kumar Joardar, Aqeeb Iqbal Arka, Janardhan Rao Doppa, and Partha Pratim Pande. 3d++: Unlocking the next generation of high-performance and energy-efficient architectures using m3d integration. In *DATE*, 2021.
- [52] Meenatchi Jagasivamani, Candace Walden, Devesh Singh, Luyi Kang, Shang Li, Mehdi Asnaashari, Sylvain Dubois, Bruce Jacob, and Donald Yeung. Memory-systems challenges in realizing monolithic computers. In *Proceedings of the International Symposium on Memory Systems*, 2018.
- [53] Srivatsa Srinivasa, Akshay Krishna Ramanathan, Xueqing Li, Wei-Hao Chen, Fu-Kuo Hsueh, Chih-Chao Yang, Chang-Hong Shen, Jia-Min Shieh, Sumeet Gupta, Meng-Fan Marvin Chang, Swaroop Ghosh, Jack Sampson, and Vijaykrishnan Narayanan. A monolithic-3d sram design with enhanced robustness and in-memory computation support. In *ISLPED*, 2018.
- [54] Srivatsa Srinivasa, Wei-Hao Chen, Yung-Ning Tu, Meng-Fan Chang, Jack Sampson, and Vijaykrishnan Narayanan. Monolithic-3d integration augmented design techniques for computing in srams. In *2019 IEEE International Symposium on Circuits and Systems (ISCAS)*, pages 1–5. IEEE, 2019.
- [55] Srivatsa Srinivasa, Yung-Ning Tu, Xin Si, Cheng-Xin Xue, Chun-Ying Lee, Fu-Kuo Hsueh, Chane-Hone Shen, Jia-Min Shieh, Wen-Kuan Yeh, Akshay Krishna Ramanathan, Mon-Shu Ho, Jack Sampson, Meng-Fan Chang, and Vijaykrishnan Narayanan. Monolithic 3d+-ic based reconfigurable compute-in-memory sram macro. In *2019 Symposium on VLSI Technology*, pages T32–T33. IEEE, 2019.
- [56] Joonho Kong, Young-Ho Gong, and Sung Woo Chung. Architecting large-scale sram arrays with monolithic 3d integration. In *2017 IEEE/ACM International Symposium on Low Power Electronics and Design (ISLPED)*, pages 1–6. IEEE, 2017.
- [57] Abdallah M. Felfl, Kamalika Datta, Arko Dutt, Hasita Veluri, Ahmed Zaky, Aaron Voon-Yew Thean, and Mohamed M. Sabry Aly. Quantifying the benefits of monolithic 3d computing systems enabled by tft and rram. In *Proceedings of the 23rd Conference on Design, Automation and Test in Europe, DATE '20*, page 43–48, 2020.
- [58] Ye Yu and Niraj K Jha. Spring: A sparsity-aware reduced-precision monolithic 3d cnn accelerator architecture for training and inference. *IEEE Transactions on Emerging Topics in Computing*, 2020.
- [59] Sho Ko, Yun Joon Soh, and Jishen Zhao. Efficient implementation of multi-channel convolution in monolithic 3d rram crossbar. *arXiv*, 2020.
- [60] Yu Huang, Long Zheng, Xiaofei Liao, Hai Jin, Pengcheng Yao, and Chuangyi Gui. Ragra: Leveraging monolithic 3d rram for massively-parallel graph processing. In *2019 Design, Automation & Test in Europe Conference & Exhibition (DATE)*, pages 1273–1276. IEEE, 2019.
- [61] Muhammad Abdullah Hanif, Aditya Manglik, and Muhammad Shafique. Resistive crossbar-aware neural network design and optimization. *IEEE Access*, 2020.
- [62] Tony F Wu, Haitong Li, Ping-Chen Huang, Abbas Rahimi, Jan M Rabaey, H-S Philip Wong, Max M Shulaker, and Subhasish Mitra. Brain-inspired computing exploiting carbon nanotube fets and resistive ram: Hyperdimensional computing case study. In *2018 IEEE International Solid-State Circuits Conference (ISSCC)*, pages 492–494. IEEE, 2018.
- [63] Tony F Wu, Haitong Li, Ping-Chen Huang, Abbas Rahimi, Gage Hills, Bryce Hodson, William Hwang, Jan M Rabaey, H-S Philip Wong, Max M Shulaker, and Subhasish Mitra. Hyperdimensional computing exploiting carbon nanotube fets, resistive ram, and their monolithic 3d integration. *IEEE Journal of Solid-State Circuits*, 53(11):3183–3196, 2018.
- [64] Emil Talpes and Diana Marculescu. Execution cache-based microarchitecture for power-efficient superscalar processors. *IEEE Transactions on Very Large Scale Integration (VLSI) Systems*, 13(1):14–26, 2005.
- [65] Baruch Solomon, Avi Mendelson, Ronny Ronen, Doron Orenstien, and Yoav Almog. Micro-operation cache: A power aware frontend for variable instruction length isa. *IEEE Transactions on Very Large Scale Integration (VLSI) Systems*, 11(5):801–811, 2003.
- [66] Daniel Sanchez and Christos Kozyrakis. ZSim: Fast and Accurate Microarchitectural Simulation of Thousand-Core Systems. In *ISCA '13*.
- [67] Makoto Motoyoshi. Through-Silicon Via (TSV). *Proceedings of the IEEE*, 2009.
- [68] Onur Mutlu, Saugata Ghose, Juan Gómez-Luna, and Rachata Ausavarungnirun. A Modern Primer on Processing in Memory. *Emerging Computing: From Devices to Systems - Looking Beyond Moore and Von Neumann*, 2021.
- [69] J. Ahn, S. Hong, S. Yoo, O. Mutlu, and K. Choi. A Scalable Processing-in-memory Accelerator for Parallel Graph Processing. In *ISCA '15*.
- [70] Amirali Boroumand, Saugata Ghose, Youngsok Kim, Rachata Ausavarungnirun, Eric Shiu, Rahul Thakur, Daehyun Kim, Aki Kuusela, Allan Knies, Parthasarathy Ranganathan, and Onur Mutlu. Google Workloads for Consumer Devices: Mitigating Data Movement Bottlenecks. In *ASPLOS '18*.
- [71] Amirali Boroumand, Saugata Ghose, Minesh Patel, Hasan Hassan, Brandon Lucia, Rachata Ausavarungnirun, Kevin Hsieh, Nastaran Hajinazar, Krishna T Malladi, Hongzhong Zheng, and Onur Mutlu. CoNDA: Efficient Cache Coherence Support for Near-Data Accelerators. In *ISCA '19*.
- [72] Kevin Hsieh, Samira Khan, Nandita Vijaykumar, Kevin K Chang, Amirali Boroumand, Saugata Ghose, and Onur Mutlu. Accelerating Pointer chasing in 3D-stacked Memory: Challenges, Mechanisms, Evaluation. In *ICCD '16*.
- [73] Ravi Nair, Samuel F Antao, Carlo Bertolli, Pradip Bose, Jose R Brunheroto, Tong Chen, C-Y Cher, Carlos HA Costa, Jun Doi, and Constantinos Evangelinos. Active Memory Cube: A Processing-in-memory Architecture for Exascale Systems. *IBM Journal of Research and Development*, '15.
- [74] Lifeng Nai, Ramyad Hadidi, Jaewoong Sim, Hyojong Kim, Pranith Kumar, and Hyesoon Kim. GraphPIM: Enabling Instruction-Level PIM Offloading in Graph Computing Frameworks. In *HPCA '17*.
- [75] Seongguk Kim, Subin Kim, Kyungjun Cho, Taein Shin, Hyunwook Park, Daehwan Lho, Shinyoung Park, Kyungjune Son, Gapeol Park, Seungtaek Jeong, Youngwoo Kim, and Joungho Kim. Signal integrity and computing performance analysis of a processing-in-memory of high bandwidth memory (pim-hbm) scheme. *IEEE Transactions on Components, Packaging and Manufacturing Technology*, 2021.
- [76] Lingjun Zhu, Lennart Bamberg, Sai Surya Kiran Pentapati, Kyungwook Chang, Francky Cathoor, Dragomir Milojevic, Manu Komalan, Brian Cline, Saurabh Sinha, Xiaoqing Xu, et al. High-performance logic-on-memory monolithic 3-d ic designs for arm cortex-a processors. *IEEE Transactions on Very Large Scale Integration (VLSI) Systems*, 2021.
- [77] Yijun Li, Jianshi Tang, Bin Gao, Jian Yao, Yue Xi, Yuankun Li, Tingyu Li, Ying Zhou, Zhengwu Liu, Qingtian Zhang, et al. Monolithic 3d integration of logic, memory and computing-in-memory for one-shot learning. In *2021 IEEE International Electron Devices Meeting (IEDM)*. IEEE, 2021.
- [78] Akifumi Kawahara, Ryotaro Azuma, Yuuichirou Ikeda, Ken Kawai, Yoshikazu Katoh, Yukio Hayakawa, Kiyotaka Tsuji, Shinichi Yoneda, Atsushi Himeno, Kazuhiko Shimakawa, Takeshi Takagi, Takumi Mikawa, and Aono Kunitoshi. An 8 mb multi-layered cross-point rram macro with 443 mb/s write throughput. *IEEE Journal of Solid-State Circuits*, 48(1):178–185, 2012.
- [79] Chung-Cheng Chou, Zheng-Jun Lin, Pei-Ling Tseng, Chih-Feng Li, Chih-Yang Chang, Wei-Chi Chen, Yu-Der Chih, and Tsung-Yung Jonathan Chang. An n40 256kx44 embedded rram macro with sl-precharge sa and low-voltage current limiter to improve read and write performance. In *2018 IEEE International Solid-State Circuits Conference (ISSCC)*, pages 478–480. IEEE, 2018.
- [80] Joseph Redmon. Darknet: Open Source Neural Networks in C. <http://pjreddie.com/darknet>, 2013.
- [81] Julian Shun and Guy E Blelloch. Lagra: A Lightweight Graph Processing Framework for Shared Memory. In *PPoPP*, 2013.
- [82] John D. McCalpin. STREAM: Sustainable Memory Bandwidth in High Performance Computers. Technical report, University of Virginia, 1991-2007. A continually updated technical report. <http://www.cs.virginia.edu/stream/>.
- [83] Shuai Che, Michael Boyer, Jiayuan Meng, David Tarjan, Jeremy W Sheaffer, Sang-Ha Lee, and Kevin Skadron. Rodinia: A Benchmark Suite for Heterogeneous Computing. In *IISWC '09*.
- [84] Steven Cameron Woo, Moriyoshi Ohara, Evan Torrie, Jaswinder Pal Singh, and Anoop Gupta. The SPLASH-2 Programs: Characterization and Methodological Considerations. *ISCA '95*.
- [85] Louis-Noël Pouchet. Polybench: The Polyhedral Benchmark Suite. [URL: http://www.cs.ucla.edu/pouchet/software/polybench](http://www.cs.ucla.edu/pouchet/software/polybench), 2012.
- [86] Christian Bienia, Sanjeev Kumar, Jaswinder Pal Singh, and Kai Li. The PARSEC Benchmark Suite: Characterization and Architectural Implications. In *PACT '08*.
- [87] Mindy D Bishop, Gage Hills, Tathagata Srimani, Christian Lau, Denis Murphy, Samuel Fuller, Jefford Humes, Anthony Ratkovich, Mark Nelson, and Max M Shulaker. Fabrication of carbon nanotube field-effect transistors in commercial silicon manufacturing facilities. *Nature Electronics*, 2020.
- [88] Devesh Singh and Donald Yeung. Morse: Memory overwrite time guided soft writes to improve rram energy and endurance. In *Proceedings of the 2024 International Conference on Parallel Architectures and Compilation Techniques*, pages 26–39, 2024.
- [89] Andrew M Bartolo, Mohamed M Sabry Aly, George Michelogiannakis, and Subhasish Mitra. Mc-elm: Multi-chip endurance-limited memory management. In *Proceedings of the International Symposium on Memory Systems*, 2023.
- [90] Geraldo F Oliveira, Juan Gómez-Luna, Lois Orosa, Saugata Ghose, Nandita Vijaykumar, Ivan Fernandez, Mohammad Sadrosadati, and Onur Mutlu. Damov:

A new methodology and benchmark suite for evaluating data movement bottlenecks. *arXiv preprint arXiv:2105.03725*, 2021.

- [91] Ahmad Yasin. A Top-Down Method for Performance Analysis and Counters Architecture. In *ISPASS '14*.
- [92] Svilen Kanev, Juan Pablo Darago, Kim Hazelwood, Parthasarathy Ranganathan, Tipp Moseley, Gu-Yeon Wei, and David Brooks. Profiling a Warehouse-Scale Computer. In *ISCA*, 2015.
- [93] Utku Sirin, Ahmad Yasin, and Anastasia Ailamaki. A Methodology for OLTP Micro-Architectural Analysis. In *DAMON*, 2017.
- [94] R. Appuswamy, J. Fellay, and N. Chaturvedi. Sequence Alignment Through the Looking Glass. In *IPDPSW*, 2018.
- [95] Intel. Intel VTune Amplifier 2019 User Guide, 2018. <https://software.intel.com/en-us/vtune-amplifier-help>.
- [96] S. Ghose, T. Li, N. Hajinazar, D. Senol Cali, and O. Mutlu. Demystifying Complex Workload-DRAM Interactions: An Experimental Study. In *SIGMETRICS*, 2020.
- [97] Vikram Sharma Mailthody, Zaid Qureshi, Weixin Liang, Ziyang Feng, Simon Garcia De Gonzalo, Youjie Li, Hubertus Franke, Jinjun Xiong, Jian Huang, and Wen-mei Hwu. Deepstore: In-storage acceleration for intelligent queries. In *Proceedings of the 52nd Annual IEEE/ACM International Symposium on Microarchitecture*, pages 224–238, 2019.
- [98] Po-An Tsai, Changping Chen, and Daniel Sanchez. Adaptive Scheduling for Systems with Asymmetric Memory Hierarchies. In *MICRO '18*.
- [99] Tse-Yu Yeh and Yale N Patt. Two-level adaptive training branch prediction. In *MICRO*, 1991.
- [100] André Seznec. Tage-sc-l branch predictors again. In *5th JILP Workshop on Computer Architecture Competitions: Championship Branch Prediction*, 2016.
- [101] Jack Choquette, Wishwesh Gandhi, Olivier Giroux, Nick Stam, and Ronny Krashinsky. NVIDIA A100 Tensor Core GPU: Performance and Innovation. *IEEE Micro*, 2021.
- [102] Aydin O Balkan, Gang Qu, and Uzi Vishkin. Mesh-of-trees and alternative interconnection networks for single-chip parallelism. *IEEE Transactions on Very Large Scale Integration (VLSI) Systems*, 17(10):1419–1432, 2009.
- [103] Jacob Benesty, Jingdong Chen, Yiteng Huang, and Israel Cohen. Pearson correlation coefficient. In *Noise reduction in speech processing*, 2009.
- [104] Taeho Kgil, Shaun D'Souza, Ali Saidi, Nathan Binkert, Ronald Dreslinski, Trevor Mudge, Steven Reinhardt, and Krisztian Flautner. Picoserver: using 3d stacking technology to enable a compact energy efficient chip multiprocessor. In *Proceedings of the 12th international conference on Architectural support for programming languages and operating systems*, pages 117–128, 2006.
- [105] Taeho Kgil, Ali Saidi, Nathan Binkert, Steve Reinhardt, Krisztian Flautner, and Trevor Mudge. Picoserver: Using 3d stacking technology to build energy efficient servers. *ACM Journal on Emerging Technologies in Computing Systems (JETC)*, 4(4):1–34, 2008.
- [106] Tudor David, Rachid Guerraoui, and Vasileios Trigonakis. Everything you always wanted to know about synchronization but were afraid to ask. In *Proceedings of the Twenty-Fourth ACM Symposium on Operating Systems Principles*, pages 33–48, 2013.
- [107] Tudor David. Libslock. URL: <https://github.com/tudordavid/liblock>.
- [108] Sheng Li, Jung Ho Ahn, Richard D Strong, Jay B Brockman, Dean M Tullsen, and Norman P Jouppi. Mcpat: An integrated power, area, and timing modeling framework for multicore and manycore architectures. In *Proceedings of the 42nd Annual IEEE/ACM International Symposium on Microarchitecture*, pages 469–480, 2009.
- [109] Stephen W Keckler, William J Dally, Daniel Maskit, Nicholas P Carter, Andrew Chang, and Whay S Lee. Exploiting fine-grain thread level parallelism on the mit multi-alu processor. *ACM SIGARCH Computer Architecture News*, 26(3):306–317, 1998.
- [110] Christina Giannoula, Nandita Vijaykumar, Nikela Papadopoulou, Vasileios Karakostas, Ivan Fernandez, Juan Gómez-Luna, Lois Orosa, Nectarios Koziris, Georgios Goumas, and Onur Mutlu. Syncron: Efficient synchronization support for near-data-processing architectures. In *2021 IEEE International Symposium on High-Performance Computer Architecture (HPCA)*, pages 263–276. IEEE, 2021.
- [111] Emil Talpes and Diana Marculescu. Power reduction through work reuse. In *Proceedings of the 2001 international symposium on Low power electronics and design*, pages 340–345, 2001.
- [112] Shruti Padmanabha, Andrew Lukefahr, Reetuparna Das, and Scott Mahlke. Dynamos: Dynamic schedule migration for heterogeneous cores. In *Proceedings of the 48th International Symposium on Microarchitecture*, pages 322–333, 2015.
- [113] Shruti Padmanabha, Andrew Lukefahr, Reetuparna Das, and Scott Mahlke. Mirage cores: The illusion of many out-of-order cores using in-order hardware. In *Proceedings of the 50th Annual IEEE/ACM International Symposium on Microarchitecture*, pages 745–758, 2017.
- [114] Xulong Tang, Orhan Kislal, Mahmut Kandemir, and Mustafa Karakoy. Data movement aware computation partitioning. In *MICRO '17*.
- [115] Shuang Chen, Yi Jiang, Christina Delimitrou, and José F Martínez. Pimcloud: Qos-aware resource management of latency-critical applications in clouds with processing-in-memory. In *2022 IEEE International Symposium on High-Performance Computer Architecture (HPCA)*. IEEE, 2022.
- [116] RM Radway, K Sethi, W-C Chen, J Kwon, S Liu, TF Wu, E Beigne, MM Shulaker, H-SP Wong, and S Mitra. The future of hardware technologies for computing: N3xt 3d mosaic, illusion scaleup, co-design. In *2021 IEEE International Electron Devices Meeting (IEDM)*, pages 25–4. IEEE, 2021.
- [117] Madhava Sarma Vemuri and Umamaheswara Rao Tida. Efficient and scalable miv-transistor with extended gate in monolithic 3d integration. In *2023 IEEE 66th International Midwest Symposium on Circuits and Systems (MWSCAS)*, pages 187–191. IEEE, 2023.
- [118] Om Prakash, Kai Ni, and Hussam Amrouch. Monolithic 3d integrated beol dual-port ferroelectric fet to break the tradeoff between the memory window and the ferroelectric thickness. In *2023 IEEE International Reliability Physics Symposium (IRPS)*, pages 1–4. IEEE, 2023.
- [119] Madhava Sarma Vemuri and Umamaheswara Rao Tida. Fdsoi process based miv-transistor utilization for standard cell designs in monolithic 3d integration. In *2023 IEEE 36th International System-on-Chip Conference (SOCC)*, pages 1–6. IEEE, 2023.
- [120] Kuangye Lu, Jaewoo Shim, Ki Seok Kim, Sang Won Kim, and Jeewan Kim. 2d materials can unlock single-crystal-based monolithic 3d integration. *Nature Electronics*, 7(6):416–418, 2024.
- [121] Maosong Xie, Yueyang Jia, Chen Nie, Zuheng Liu, Alvin Tang, Shiquan Fan, Xiaoyao Liang, Li Jiang, Zhezhi He, and Rui Yang. Monolithic 3d integration of 2d transistors and vertical rams in 1t–4r structure for high-density memory. *Nature Communications*, 14(1):5952, 2023.
- [122] Shi-Xian Guan, Tilo H Yang, Chih-Hao Yang, Chuan-Jie Hong, Bor-Wei Liang, Kristan Bryan Simbulan, Jyun-Hong Chen, Chun-Jung Su, Kai-Shin Li, Yuan-Liang Zhong, et al. Monolithic 3d integration of back-end compatible 2d material fet on si finfet. *npj 2D Materials and Applications*, 2023.
- [123] Jun-young Kim, Xin Ju, Kah-Wee Ang, and Dongzhi Chi. Van der waals layer transfer of 2d materials for monolithic 3d electronic system integration: review and outlook. *ACS nano*, 17(3):1831–1844, 2023.
- [124] Rahul Pendurthi, Najam U Sakib, Muhtasim Ul Karim Sadaf, Zhiyu Zhang, Yongwen Sun, Chen Chen, Darsith Jayachandran, Aaryan Oberoi, Subir Ghosh, Shalini Kumari, et al. Monolithic three-dimensional integration of complementary two-dimensional field-effect transistors. *Nature nanotechnology*, 19(7):970–977, 2024.
- [125] Yiwei Du, Jianshi Tang, Yijun Li, Yue Xi, Bin Gao, He Qian, and Huaqiang Wu. Monolithic 3d integration of fefet, hybrid cmos logic and analog rram array for energy-efficient reconfigurable computing-in-memory architecture. In *VLSI Technology and Circuits*. IEEE, 2023.
- [126] Tathagata Srimani, Robert M Radway, Jinwoo Kim, Kartik Prabhu, Dennis Rich, Carlo Gilardi, Priyanka Raina, Max Shulaker, Sung Kyu Lim, and Subhasish Mitra. Ultra-dense 3d physical design unlocks new architectural design points with large benefits. In *DATE*, 2023.
- [127] Fan Chen, Linghao Song, Hai Li, and Yiran Chen. Marvel: A vertical resistive accelerator for low-power deep learning inference in monolithic 3d. In *2021 Design, Automation & Test in Europe Conference & Exhibition (DATE)*. IEEE, 2021.
- [128] Ji-Hoon Kang, Heechang Shin, Ki Seok Kim, Min-Kyu Song, Doyoon Lee, Yuan Meng, Chanyeol Choi, Jun Min Suh, Beom Jin Kim, Hyunseok Kim, et al. Monolithic 3d integration of 2d materials-based electronics towards ultimate edge computing solutions. *Nature materials*, 2023.
- [129] Shubham Kumar, Paul R Genssler, Somaya Mansour, Yogesh Singh Chauhan, and Hussam Amrouch. Frontiers in ai acceleration: From approximate computing to fefet monolithic 3d integration. In *IFIP/IEEE 31st International Conference on Very Large Scale Integration*. IEEE, 2023.
- [130] Ye Yu and Niraj K Jha. A monolithic 3d hybrid architecture for energy-efficient computation. *IEEE Transactions on Multi-Scale Computing Systems*, 2018.
- [131] Jiaming Li, Bin Gao, Ruihua Yu, Peng Yao, Jianshi Tang, He Qian, and Huaqiang Wu. A spatial-designed computing-in-memory architecture based on monolithic 3d integration for high-performance systems. In *ACM International Symposium on Nanoscale Architectures*, 2023.
- [132] Yibei Zhang, Yijun Li, Jianshi Tang, Ningfei Gao, Lei Gao, Haitao Xu, Ran An, Qi Qin, Zhengwu Liu, Dong Wu, et al. 3d stackable cntfet/rram 1t1r array with cnt cmos peripheral circuits as beol buffer macro for monolithic 3d integration with analog rram-based computing-in-memory. In *2023 International Electron Devices Meeting (IEDM)*, pages 1–4. IEEE, 2023.
- [133] AMD. AMD Accelerating – The High Performance Computing Ecosystem, 2021. <https://www.amd.com/en/events/computex>.
- [134] Amna Shahab, Mingcan Zhu, Artemiy Margaritov, and Boris Grot. Farewell My Shared LLC! A Case for Private Die-Stacked DRAM Caches for Servers. In *MICRO*, 2018.